

To Appear in **The Astrophysical Journal**, Vol. **471**, 1996

Chaos and Mixing in Triaxial Stellar Systems

David Merritt and Monica Valluri¹

Department of Physics and Astronomy, Rutgers University, New Brunswick, NJ 08855

ABSTRACT

We investigate the timescales for stochasticity and chaotic mixing in a family of triaxial potentials that mimic the distribution of light in elliptical galaxies. Some of the models include central point masses designed to represent nuclear black holes. Most of the boxlike orbits are found to be stochastic, with mean Liapunov times that are 3 – 6 times the period of the long-axis orbit. In models with large cores or small black holes, the stochastic orbits mimic regular box orbits for hundreds of oscillations at least. However a small core radius or significant black hole mass causes most of the stochastic orbits to diffuse through phase space on the same timescale, visiting a significant fraction of the volume beneath the equipotential surface. Some stochastic orbits, with initial conditions lying close to those of regular orbits, remain trapped in all models.

We estimate timescales for chaotic mixing in the more strongly stochastic models by evolving ensembles of 10^4 points until their distribution reaches a nearly steady state. Mixing initially takes place rapidly, with characteristic times of 10 – 30 dynamical times, as the phase points fill a region similar in shape to that of a box orbit. Subsequent mixing is slower, with characteristic times of hundreds of orbital periods. Mixing rates were found to be enhanced by the addition of modest force perturbations, and we propose that the stochastic parts of phase space might be efficiently mixed during the early phases of galaxy formation when such perturbations are large. The consequences for the structure and evolution of elliptical galaxies are discussed.

1. Introduction

Elliptical galaxies appear to be smooth and well-ordered systems, and this apparent regularity is often taken as evidence for an underlying mathematical simplicity. Jeans

¹Current address: Department of Astronomy, Columbia University, New York, NY 10027

(1915) first showed how to construct analytic models of time-independent galaxies based on forms for the gravitational potential that support only regular, i.e. non-chaotic, stellar orbits. Jeans’s theorem has motivated a large number of studies based on assumed forms for the gravitational potential in which the motion is characterized by two or more global invariants. For instance, all the trajectories in a spherically-symmetric potential respect four isolating integrals of the motion, and in axisymmetric potentials both the energy E and angular momentum about the symmetry axis L_z are globally conserved. Motion in a spherical potential is therefore fully regular, and any chaotic orbits in an axisymmetric potential must remain confined to a phase space region of constant E and L_z . It is common practice in modelling axisymmetric systems to assume that the phase space density is constant on surfaces of constant E and L_z so that the chaos, if present, is simply ignored.

This picture changes somewhat when we consider less symmetrical forms for the potential. Motion in the potential of an ellipsodially stratified mass model can be fully regular, as shown by Kuzmin (1973) and de Zeeuw & Lynden-Bell (1985), but Kuzmin’s model does not mimic very well the distribution of mass or light in real galaxies. In more general triaxial models, some orbits appear to retain three integrals of the motion while others become irregular, conserving only the energy (Merritt 1980; Udry & Pfenniger 1988). In a pioneering study, Goodman & Schwarzschild (1981) showed that a significant fraction of the orbits in the triaxial potential generated by Hubble’s (1930) density law are stochastic. However they found that the chaos was of little consequence for the orbital motion, since stochastic orbits appeared to behave very much like regular orbits over timescales of 10^2 orbital oscillations. They coined the term “semi-stochasticity” to describe this phenomenon. Since Goodman & Schwarzschild’s study, most reviews of elliptical galaxy dynamics have emphasized the near-regularity of the stochastic motion in triaxial potentials (e.g. Schwarzschild 1987; Gerhard 1993; de Zeeuw 1994).

Hints that chaos might play a larger role in elliptical galaxy dynamics appeared in Schwarzschild’s (1993) study of scale-free, $\rho \propto r^{-2}$, triaxial models. Schwarzschild found that most of the boxlike orbits in each of six scale-free models were stochastic. The exceptions were orbits lying near to stable periodic orbits, or “boxlets,” that avoided the center. At the same time, it became clear that the distribution of light in early-type galaxies is better described by Schwarzschild’s scale-free models than by the models of Hubble (1930) or Kuzmin (1973) with their large, constant-density cores. High-resolution observations revealed that elliptical galaxies never have cores; instead, the luminosity density always increases monotonically toward the center (Crane et al. 1993; Ferrarese et al. 1994; Moller, Stiavelli & Zeilinger 1995; Lauer et al. 1995). Even elliptical galaxies that were once thought to have well-resolved cores, like M87, are now known to contain cusps with a weak, power-law dependence of density on radius (Merritt & Fridman 1995;

Gebhardt et al. 1996). In addition, there is increasingly strong evidence for central mass concentrations, possibly supermassive black holes, at the centers of many early-type galaxies (Ford et al. 1994; Miyoshi et al. 1995). Some nearby galaxies like M32 exhibit both steep central cusps and pointlike central mass concentrations (Tonry 1987).

The motion of boxlike orbits in triaxial models with central mass concentrations is often strongly chaotic. Gerhard & Binney (1985) investigated the two-dimensional motion of stars in potentials with central point masses and steep density cusps. They found that central singularities can subject stars on boxlike orbits to deflections that destroy their nonclassical integrals of motion. The evolution of such an orbit can be described as a series of near-random transitions from one box orbit to another. Merritt & Fridman (1996) computed libraries of orbits in two triaxial models with Dehnen’s (1993) density law:

$$\rho(m) = \rho_0 m^{-\gamma} (1 + m)^{-(4-\gamma)}, \quad m^2 = \frac{x^2}{a^2} + \frac{y^2}{b^2} + \frac{z^2}{c^2} \quad (1)$$

with $\gamma = 1$ (“weak cusp”) and $\gamma = 2$ (“strong cusp”). They found a similar, large fraction of stochastic orbits in both potentials but the behavior of these orbits was different in the two cases. In the weak-cusp potential, almost all of the stochastic orbits mimicked regular boxlike orbits for more than 10^2 oscillations – roughly the same behavior seen by Goodman & Schwarzschild (1981) in their triaxial model with a large core. In the strong-cusp potential, however, the stochastic orbits appeared to diffuse over the energy surface on timescales of only $10^2 - 10^3$ oscillations. After that time, most of the stochastic orbits in the strong-cusp model had reached a time-averaged steady state that was approximately the same for all stochastic orbits at a given energy – the orbits had essentially filled the “Arnold web” (Arnold 1964). The replacement of distinguishable stochastic orbits by these time-invariant ensembles reduces substantially the freedom to construct self-consistent equilibria, and in fact Merritt & Fridman (1996) could find no fully stationary solution corresponding to the strong-cusp model.

These studies suggest that chaos is a common consequence of triaxiality, and furthermore that the timescales over which the chaos manifests itself in the orbital motion can be physically interesting – long compared to a crossing time, but often (and especially near the center) short compared to a Hubble time. In this paper we attempt to more accurately calculate these timescales. Our goal is to understand the role that stochasticity plays in the structure and evolution of early-type galaxies. If the timescale for chaotic orbits to fill their allowed phase space is short compared to the age of a galaxy, stochasticity could strongly reduce the variety of orbits available for the construction of equilibrium galaxies. This in turn might imply that triaxiality is a rare phenomenon (Schwarzschild 1981). On the other hand, if chaotic timescales are similar to or greater than a galaxy lifetime, triaxial

galaxies might be slowly evolving as the stochastic orbits continue to diffuse — an equally interesting possibility.

We investigate these questions by integrating ensembles of orbits in a family of triaxial models that mimic the distribution of light in early-type galaxies. Our family (§2) contains Kuzmin’s integrable model as a special case. By varying a free parameter, m_0 , we can change the size of the constant-density region near the center; for $m_0 = 0$, our models have a $\rho \propto r^{-2}$ central cusp similar to those observed in some early-type galaxies. We are thus able to study the way in which departures from perfect integrability ($m_0 = 1$) induce stochasticity in the motion. We find (§3) that the number of stochastic orbits is not a strong function of m_0 , and that the typical Liapunov exponent is $0.1 - 0.3$ in units of the inverse dynamical time (defined as the full period of the long-axis orbit). Some of the stochastic orbits appear to mimic regular orbits for hundreds of oscillations or even longer. This “trapping” affects virtually all of the stochastic orbits in the potentials with large m_0 , but is much less important as $m_0 \rightarrow 0$, and most of the stochastic orbits in the cuspy models behave ergodically over astronomical timescales (§4).

Although our calculations are restricted to motion in a single family of triaxial models, our results are relevant to a broader question. How do galaxies reach a steady state? Jeans’s theorem requires that the phase-space density f be constant on the tori that define the range of motion of the regular orbits. But it is well known that the evolution of a collisionless ensemble of stars is never toward the uniform population of phase space demanded by Jeans’s theorem. Any initially compact group of phase points gets drawn out into a filament of ever-decreasing width as they move independently in response to the gravitational force. Observed with infinite resolution, the phase space occupied by these points becomes increasingly striated, not more uniform. The most we can hope for is that the coarse-grained phase space density will approach a constant value within some region; but even this outcome is not guaranteed by any general property of Hamilton’s equations.

One mechanism by which an ensemble of regular trajectories can evolve to a coarse-grained steady state is phase mixing. A simple example of phase mixing is a set of stars on circular orbits with the same initial phase, $f_0(r, \phi) = \delta(\phi - \phi_0)$, $r_1 < r < r_2$. If the circular frequency Ω is a function of radius, this sliver will be wound into a filament (Figure 1a); the Fourier coefficients of the distribution in configuration space will be

$$A_k \propto \int_{r_1}^{r_2} dr r^2 \int_0^{2\pi} d\phi \cos k\phi \delta[\phi - \Omega(r)t] \quad (2)$$

$$\propto \int_{r_1}^{r_2} dr r^2 \cos[k\Omega(r)t]. \quad (3)$$

For any smoothly-varying $\Omega(r)$, the Riemann-Lebesgue theorem guarantees that at late times $A_k \rightarrow 0$ for $k \neq 0$. Thus the coarse-grained density, i.e. the density averaged over

some radial interval, tends to a value that is independent of angle even though the density of points on any particular orbit is nonzero only at a single value of ϕ .

Phase mixing undoubtedly plays a role in the approach of collisionless stellar systems to equilibrium. But phase mixing is an intrinsically slow process – in fact it has no well-defined timescale. The rate at which a group of phase points shears depends on the range of orbital frequencies in the group. If the maximum and minimum frequencies are Ω_1 and Ω_2 respectively, we expect phase mixing to take place on a timescale of order $(\Omega_1 - \Omega_2)^{-1}$. This timescale is never less than a dynamical time and can be much longer. For instance, near the half-mass radius r_e of a de Vaucouleurs-law galaxy, the phase mixing time $2\pi/(\Omega_1 - \Omega_2)$ for two stars on circular orbits with separation Δr is roughly $0.85/(\Delta r/r_e)$ times the orbital period. Inhomogeneities on a scale of $0.1r_e$ – roughly 100 pc in a real galaxy – damp out over ~ 10 dynamical times, and shorter length scales reach equilibrium even more slowly. In the limit $\Omega_1 \rightarrow \Omega_2$ there is no phase mixing. This is the case for a set of points that is restricted to a single invariant torus: the ensemble simply translates, with fixed shape, around the torus as the phase points move with the same fixed set of frequencies.

Phase mixing is also limited in the sense that it can only reshuffle phase points within a narrow region, since by definition the trajectories are confined to invariant tori. Mixing in a system with a time-evolving potential, or in a system containing irregular orbits, must operate via some different mechanism.

Returning to the example discussed above, we can ask: what property of the motion guarantees the vanishing, after long times, of the Fourier components of f ? The periodicity of the motion with respect to time is clearly sufficient for this purpose, but it is not necessary. One could imagine more general flows for which the coarse-grained density converges to a form that is independent of angle. In fact any motion which has the property that the average time spent in any phase interval $d\phi$ is proportional to $d\phi$ will do the trick, since at late times ϕ will have no preferred value at any radius. This includes flows that are discontinuous, or even random, with respect to time. We will follow the now-standard practice of calling “ergodic” any motion that spends equal amounts of time, on average, in equal phase-space volumes (defined with respect to the invariant measure).² Ergodicity is a non-trivial property of dynamical systems; it is characteristic of quasi-periodic motion, i.e. regular orbits (Arnold 1989, p. 287), but other types of motion can be ergodic as well.

²The term ergodic was originally used to describe motion that visits every point on the energy surface. Modern usage recognizes the fact that this stringent condition is rarely satisfied in real systems, and hence that ergodicity is more usefully defined over some limited part of the energy surface, such as an invariant torus (Lichtenberg & Lieberman 1983, p.260).

While ergodicity is a necessary property of the motion if phase mixing is to produce a steady state, ergodicity by itself is a condition only on the time-averaged behavior of a trajectory. Relaxation implies more in general: not only should the entire past of a given phase point cover the phase space uniformly, but so also should the present of any neighborhood of the original point. In other words, any small patch of phase space should evolve in such a way that it uniformly covers, at a *single* later time, a much larger region. Motion that is restricted to a single torus, while ergodic, does not have this stronger property, since a collection of phase points simple translates unchanged around the torus. Phase mixing, which involves points on different tori, does produce a weak sort of relaxation but only within the narrow region allowed by the integrals of motion.

Dynamicists define as “mixing” any system which exhibits this stronger form of relaxation. A standard definition of a mixing system (e.g. Lichtenberg & Lieberman 1983, p. 268) is one in which any portion of the phase space, however small, tends to be uniformly distributed over the energy surface (or some subspace defined by the integrals of motion) as the time increases indefinitely (Fig. 1b). Mixing systems are always ergodic (Arnold & Avez 1968), but the converse is not true; for instance, motion on the torus is ergodic but not mixing. Mixing systems have the further property that they relax: the density in a mixing system evolves toward a constant, coarse-grained value at all accessible phase space points. The trajectories in mixing systems are often stochastic, since stochasticity guarantees the drastic loss of correlations that is required if relaxation is to erase memory of the initial state. In fact the canonical examples of mixing systems, such as the hard-sphere gas (Sinai 1976), are fully chaotic systems. Mixing also has an associated timescale (Krylov 1979); in this sense too it differs from phase mixing for which no characteristic time can be defined.

A mixing flow has many of the properties that we associate with the approach to equilibrium of collisionless stellar systems. The mixing property has been rigorously proved only for a small set of idealized, strongly chaotic dynamical systems (Ott 1993, p. 257). In potentials containing both regular and stochastic orbits, like those of galaxies, we intuitively expect that the stochastic orbits – which are effectively random in their long-time behavior – will be both ergodic and mixing over the bounded portion of the phase space for which they exist. However the time required for the mixing to produce an equilibrium state might be long, especially if the stochastic motion is hampered by the presence of invariant tori and “cantori.” Although a proof of mixing in realistic galactic potentials would be extremely difficult, we can still hope to observe the signature of mixing behavior – approach to a characteristic, coarse-grained equilibrium on some well-defined timescale – in numerical experiments. This we do, in §5.

In a real galaxy, the approach to a steady state takes place against the backdrop of

an evolving potential. Mixing should be more efficient in this case, since energy is no longer an invariant of the motion and stars are free to move throughout the entire phase space. Furthermore a potential that is changing in a complicated way with time might induce chaotic motion, or something like it, in the particle trajectories. Although we do not attempt here to simulate this more complicated process, we do show in §5 that the addition of random force perturbations can enhance the mixing rates of stochastic ensembles. This leads us to propose that rapidly-varying forces during galaxy formation might cause the stochastic parts of phase space to be strongly mixed by the time the gravitational potential settles down. The replacement of distinguishable stochastic orbits by a smaller number of invariant ensembles would reduce the freedom to construct self-consistent equilibria; some possible consequences for real galaxies are discussed in §6.

2. A Family of Triaxial Models

In this section we identify a family of mass models that resemble real elliptical galaxies and bulges and calculate their gravitational potentials. Our starting point is the Perfect Ellipsoid (Kuzmin 1973; de Zeeuw & Lynden-Bell 1985), with mass distribution

$$\rho(m) = \frac{\rho_0}{(1 + m^2)^2}. \quad (4)$$

Motion in the gravitational potential of the Perfect Ellipsoid is characterized by three global integrals, i.e. the motion is completely regular. All orbits fall into one of four families: the boxes, and three families of tubes (Kuzmin 1973; de Zeeuw 1985). Tube orbits circulate either around the long (x) or short (z) axis of the figure, and conserve a quantity analogous to the angular momentum about that axis. They therefore avoid the center. Box orbits have filled centers and touch the equipotential surface at eight points, one in each octant.

Kuzmin's density law was arrived at via mathematical manipulations and it is not surprising that the Perfect Ellipsoid bears little resemblance to the distribution of light or mass in real elliptical galaxies. The discrepancy is particularly great near the center, where Kuzmin's law predicts a large, constant-density core. The luminosity densities in real elliptical galaxies and bulges are always observed to rise monotonically at small radii (Ferrarese et al. 1994; Moller, Stiavelli & Zeilinger 1995; Lauer et al. 1995). The steepest profiles are seen in low-luminosity galaxies like M32, while brighter galaxies like M87 have surface brightness profiles that look superficially core-like (Kormendy et al. 1995). However Merritt & Fridman (1995) showed that even these “core” galaxies have power-law cusps in the luminosity density. These galaxies appear to have cores only because the logarithmic slopes of their density cusps are less than -1 , and a shallow power law cusp produces a

gently curving surface brightness profile when seen projected through the outer layers of the galaxy (Dehnen 1993, Fig. 1).

We would like to find a simple mathematical expression for the mass distribution that reproduces, at least qualitatively, the distribution of light seen in real galaxies. Ideally our expression should contain Kuzmin’s law as a special case so that we can study the way in which departures from the Perfect law generate irregular motion. In addition, the gravitational forces generated by our model should be simple to calculate in order that the orbit integrations not be too slow.

A mass model that satisfies each of these requirements is

$$\rho(m) = \frac{\rho_0 m_0^2}{(1+m^2)(m_0^2+m^2)}, \quad 0 \leq m_0 \leq 1. \quad (5)$$

The central density ρ_0 is related to the total mass M by the expression

$$\rho_0 = \frac{M(1+m_0)}{2\pi^2 abc m_0^2}.$$

The density profile breaks into three regions (Fig. 2). At large radii, $m \gg 1$, the density falls off as m^{-4} , as in the Perfect law. At intermediate distances from the center, $m_0 \lesssim m \lesssim 1$, $\rho \sim m^{-2}$. Near the center, $m \lesssim m_0$, the density becomes constant. For $m_0 = 1$ the profile reduces to Kuzmin’s law, while for $m_0 = 0$ it has a $\rho \propto m^{-2}$ central density cusp like those observed in some elliptical galaxies. Thus varying m_0 from 1 to 0 takes one from a fully integrable but nonphysical model, to a realistic but (as we will see) strongly nonintegrable model.

We do not have the freedom with our family of models to adjust the slope of the central density cusp to any power-law index. We are therefore not able to reproduce the shallow power-law cusps observed in luminous elliptical galaxies. However in a galaxy where the density increases near the center as a power law of index γ , the radial force reaches a maximum value at some nonzero radius for $\gamma < 1$, and we might expect the motion in such a galaxy to be crudely reproducible with our models if m_0 is chosen to have an appropriate value. For instance, in a galaxy with Dehnen’s (1993) density law, $\rho \propto r^{-\gamma}(a+r)^{\gamma-4}$, the radial force peaks at $r = a(1-\gamma)/2$ for $\gamma < 1$. Thus from a dynamical point of view such a galaxy has a “core” even though the density is diverging near the center.

The gravitational potential generated by an ellipsoidally-stratified mass distribution is

$$\Phi(\mathbf{x}) = -\pi Gabc \int_0^\infty \frac{[\psi(\infty) - \psi(u)]du}{\sqrt{(u+a^2)(u+b^2)(u+c^2)}}, \quad (6)$$

(Chandrasekhar 1969, Theorem 12), where

$$\psi(m) = \int_0^{m^2} \rho(m'^2) dm'^2$$

and

$$m^2(u) = \frac{x^2}{a^2 + u} + \frac{y^2}{b^2 + u} + \frac{z^2}{c^2 + u}.$$

For the density distribution (5), we find

$$\psi(m) = \frac{1}{2\pi abc(1 - m_0)} \left[\log(1 + m^2/m_0^2) - \log(1 + m^2) \right] \quad (7)$$

and the potential becomes

$$\Phi(\mathbf{x}) = \Phi_0 - \frac{1}{2\pi(1 - m_0)} \int_0^\infty \frac{[\log(1 + m^2) - \log(1 + m^2/m_0^2)]}{\sqrt{(u + a^2)(u + b^2)(u + c^2)}} du \quad (8)$$

where

$$\Phi_0 = \frac{2 \log m_0}{\pi(1 - m_0)} R_F(a^2, b^2, c^2) \quad (9)$$

and R_F is Carlson's incomplete elliptic integral of the first kind. We have adopted units in which the total mass M , the gravitational constant G , and the long axis length a are equal to one.

Gravitational forces can be computed by taking the gradient of Eq. (8). The expressions so obtained are expensive to compute numerically, since they contain an integral which must be evaluated anew at every point along the trajectory. A better way to proceed is to make use of the fact that the density (5) can be written

$$\rho(m) = \frac{1}{2\pi^2 abc(1 - m_0)} \left[\frac{1}{m^2 + m_0^2} - \frac{1}{m^2 + 1} \right]. \quad (10)$$

De Zeeuw and Pfenniger (1988) show that the gravitational potential generated by a mass density of the form $\rho = \rho_0/(m_0^2 + m^2)$ can be expressed in terms of confocal ellipsoidal coordinates (λ, μ, ν) , defined as the three roots for u in the equation $m^2(-u) = -1$. On transforming to ellipsoidal coordinates we have

$$1 + m^2(u) = \frac{(\lambda + u)(\mu + u)(\nu + u)}{(a^2 + u)(b^2 + u)(c^2 + u)}, \quad (11)$$

and the potential becomes

$$\Phi(\mathbf{x}) = \Phi_0 - \frac{1}{2\pi(1 - m_0)} [G(\lambda) + G(\mu) + G(\nu) - m_0 (H(\lambda') + H(\nu') + H(\mu'))]. \quad (12)$$

Here (λ, μ, ν) and (λ', μ', ν') are separate sets of ellipsoidal coordinates corresponding respectively to the axis lengths (a, b, c) and (am_0, bm_0, cm_0) , and

$$G(\tau) = \int_0^\infty \frac{\log(\tau + u)du}{\sqrt{(a^2 + u)(b^2 + u)(c^2 + u)}}, \quad (13)$$

$$H(\tau') = \int_0^\infty \frac{\log(\tau' + u)du}{\sqrt{(a^2 m_0^2 + u)(b^2 m_0^2 + u)(c^2 m_0^2 + u)}}. \quad (14)$$

Furthermore it can be shown that

$$m_0 H(\tau') = G(\tau'/m_0^2) + \text{constant} \quad (15)$$

so that

$$\Phi(\mathbf{x}) = \Phi_0 - \frac{1}{2\pi(1-m_0)} \left[G(\lambda) + G(\mu) + G(\nu) - G(\lambda'/m_0^2) - G(\mu'/m_0^2) - G(\nu'/m_0^2) \right]. \quad (16)$$

This expression for the gravitational potential is not necessarily faster to evaluate numerically than the one based on Chandrasekhar's formula in Cartesian coordinates. However, the gravitational forces may now be expressed as sums of terms like

$$\frac{(\lambda - b^2)(\lambda - c^2)}{(\lambda - \mu)(\lambda - \nu)} R_J(a^2, b^2, c^2, \lambda), \quad (17)$$

with R_J Carlson's third incomplete elliptic integral. The functions R_J depend on a single argument and may be approximated via splines at the start of the integration. In this way, the calculation of orbits can be speeded up by roughly an order of magnitude without a significant loss in accuracy. The details are presented in the Appendix.

There is increasingly strong evidence for central singularities, possibly supermassive black holes, at the centers of a few early-type galaxies (Ford et al. 1994; Miyoshi et al. 1995). It is possible that most or all elliptical galaxies contain such black holes with masses in the range 0.1 – 1% the total stellar mass (Kormendy & Richstone 1995). Accordingly, we also investigate the orbital motion in triaxial models containing central point masses. The masses of these “black holes,” M_{BH} , will henceforth be expressed as fractions of the galaxy mass.

3. Liapunov Exponents

In this section we compute the simplest index of stochasticity, the Liapunov exponents, for a large number of orbits in the gravitational potential just defined. The Liapunov

exponents are interesting in their own right, as measures of the rate of divergence of nearby trajectories and as diagnostics for separating regular from stochastic orbits. But we also expect the Liapunov exponents to be related to the rate of mixing, since mixing is driven by the spreading of trajectories.

The phase space of the potential (8) is partly regular and partly stochastic. The majority of stochastic trajectories in a triaxial potential have the property that they touch the surface $\Phi(\mathbf{x}) = E$ at a set of stationary points (Schwarzschild 1993; Merritt & Fridman 1996). Our initial conditions were therefore taken to be on one octant of the equipotential surface, with zero velocity. We selected the starting points of each isoenergetic ensemble of orbits on a regular grid of 192 points distributed over the equipotential surface, as described by Merritt & Fridman (1996).

The Liapunov exponents of a trajectory are the mean exponential rates of divergence of trajectories surrounding it. In a three-degrees-of-freedom system there are six Liapunov exponents for every trajectory, corresponding to the six dimensions of phase space. The exponents come in pairs of opposite sign; of the three independent exponents, one – corresponding to displacements in the direction of the motion – is always zero. We are thus left with two independent exponents, σ_1 and σ_2 . These may be seen as defining the time-averaged divergence rates in two directions orthogonal to the trajectory. For a regular orbit, $\sigma_1 = \sigma_2 = 0$; for a stochastic orbit, at least one (and typically two) of these exponents is nonzero.

Liapunov exponents are defined as limiting values over an infinite time interval (e.g. Lichtenberg & Lieberman 1983, p. 264), and hence are impossible to calculate via any finite numerical scheme. We computed approximations to the Liapunov exponents by integrating orbits for long periods, up to 10^4 dynamical times $T_D(E)$, defined as the full period of the x -axis orbit of energy E . We used the Gram-Schmidt orthogonalization technique described by Benettin et al. (1980) in an implementation developed by the Geneva Observatory group and kindly made available by Dr. Stéphane Udry. The evolution of the perturbed orbits is determined by the second derivatives of the potential with respect to position; these expressions are given in the Appendix. The time required to integrate one orbit and its six perturbation orbits for 10^4 orbital times and compute the Liapunov exponents was about 80 minutes on a DEC Alpha 3000/700 workstation. Henceforth we will use the term “Liapunov exponents” to refer to these finite-time, numerical approximations to the true exponents.

We fixed the axis ratios of our triaxial model to $c/a = T = 0.5$, where $T = (a^2 - b^2)/(a^2 - c^2)$ is the “triaxiality index”; our choice for T corresponds to “maximum triaxiality.” We chose three values for the core radius, $m_0 = \{0.1, 0.01, 0.001\}$,

and three values for the mass of the central “black hole,” $M_{BH} = \{1, 3, 10\} \times 10^{-3}$. For comparison, the ratio of black hole mass to luminous galaxy mass is thought to be about 5×10^{-3} for M87 and 2.5×10^{-3} for M32 (Kormendy & Richstone 1995). All orbits had an energy equal to that of the long-axis orbit that just touches the ellipsoidal shell dividing the model into two equal-mass parts. The amplitude of this orbit is roughly 1 in all of the models considered here.

Figures 3-5 shows histograms of σ_1 and σ_2 for various combinations of m_0 and M_{BH} . Each plot contains three curves corresponding to integration times of 10^2 , 10^3 and $10^4 T_D$ for the same set of 192 orbits. As the integration time increases, the separation of the orbits into two groups becomes apparent. The Liapunov exponents of the regular orbits, the “boxlets” (Miralda-Escude & Schwarzschild 1989), lie in a narrow peak near zero. The Liapunov exponents of the stochastic orbits show a larger spread, but the spread decreases with time and the mean value does not change very much after $10^3 T_D$.

We expect that every stochastic orbit at a given energy moves in the same stochastic “sea,” interconnected via the Arnold web (Arnold 1964). One can begin to identify, after 10^4 dynamical times, the unique numbers $\sigma_1(E)$ and $\sigma_2(E)$ that characterize the stochastic motion in this sea. Table 1 gives Liapunov exponents in units of T_D^{-1} at $t = 10^4 T_D$ for various combinations of m_0 and M_{BH} . These values are simple averages over the subset of orbits that lie within the stochastic part of the histogram, defined to be the part to the right of the narrow peak defining the regular orbits. Also given there are the dispersions of the σ values about their means, and the number of orbits, out of the total 192, that are stochastic.

A large fraction of the non-tube orbits are stochastic, and this fraction is not tremendously dependent on m_0 or M_{BH} . Even for $m_0 = 0.1$ and $M_{BH} = 0$ — not greatly different from the Perfect Ellipsoid — about half of the equipotential surface generates stochastic orbits, and this fraction increases to $\sim 150/192$ when m_0 has the physically more realistic values of 10^{-2} or 10^{-3} . The addition of a central point mass does not increase the fraction of stochastic orbits very much. The Liapunov exponents for the most stochastic model considered here, $m_0 = 10^{-3}$ and $M_{BH} = 0.01$, are $\sigma_1 \approx 0.32$ and $\sigma_2 \approx 0.13$ in units of the inverse dynamical time. The most nearly regular model, $m_0 = 0.1$ and $M_{BH} = 0$, has mean Liapunov exponents that are only a factor of $\sim 2 - 3$ lower than these extreme values.

Roughly speaking, then, divergence between nearby stochastic orbits takes place on timescales that average 3-6 times the dynamical time in all of our models.

We found that σ_2 correlated strongly with σ_1 in our ensembles; there were few if any orbits with large σ_1 and small σ_2 . A vanishing σ_2 would imply the existence of an isolating

integral in addition to the energy. It appears that most or all of the stochastic orbits in our model potentials respect only the energy integral.

4. Trapped Orbits

Figures 3-5 give hints of a second, longer timescale associated with the stochasticity. After an infinite time (according to Arnold’s conjecture) all of the stochastic orbits in an isoenergetic ensemble should have exactly the same values of σ_1 and σ_2 . While our results are consistent with this conjecture, Figures 3-5 show that the spread in the Liapunov exponents at a given energy decreases very slowly with time, remaining appreciable even after $10^3 T_D$. Much of the spread is due to extended tails in the histograms toward low values of σ_1 and σ_2 . The slow rate at which the Liapunov exponents evolve toward a common value suggests that many stochastic orbits fail to explore the full stochastic phase space in an effectively ergodic manner. Apparently, this trapping can persist for periods of time much longer than σ_1^{-1} . Inspection of the configuration-space plots confirms this expectation. Many of the stochastic orbits are found to mimic regular boxlike orbits for hundreds of oscillations before suddenly changing to a different boxlike shape, etc. Similar behavior has been noted by many authors (e.g. Goodman & Schwarzschild 1981; Binney 1982a).

The confinement of stochastic orbits to limited parts of phase space over long periods of time is due to the fact that our phase space is “decomposable,” i.e. contains both regular and stochastic parts. In a decomposable phase space, some of the stochastic trajectories travel close to the imbedded tori and can become stuck there for a long time (e.g. Karney 1983).

We investigated the degree of trapping via the scheme described by Goodman & Schwarzschild (1981). The surface of section $E = E_0$, $x = y = z = 0$ is intersected by the majority of boxlike orbits, excluding only those that lie close to a stable resonance that avoids the center. An orbit respecting two integrals of the motion in addition to the energy will pass through this point with at most a finite set of velocity vectors, while an orbit respecting only the energy integral will not be constrained in the direction of its velocity. A trapped stochastic orbit may be distinguished from a more freely-moving one by inspecting the fraction of the velocity-space sphere that it covers after successive passages through the central point.

We constructed surfaces of section for each of the orbits in our ensembles by integrating them for a time interval of $500 T_D$ and recording their velocities at the central crossings. In

practice, this meant recording passages through the sphere $(x^2 + y^2 + z^2)^{1/2} < 0.03$. These velocities were then mapped onto one octant of the velocity-space sphere, as in Goodman & Schwarzschild (1981).

In the potential with the largest core and no black hole, $m_0 = 0.1$ and $M_{BH} = 0$, the stochastic orbits all remained confined to small regions in this surface of section. The largest scatter was produced by stochastic orbits with starting points near the $y - z$ plane and the z axis, but even these orbits covered an area only $\sim 4 - 6$ times that of a typical regular orbit on the surface of section. This behavior is similar to that described by Goodman & Schwarzschild (1981) for motion in a Hubble-law potential. It is also consistent with the histograms of Figure 3, which show considerable spread in the Liapunov exponents of the orbits in this model even after $10^3 T_D$.

When m_0 was decreased to 10^{-2} or 10^{-3} , however, the scatter in the surface of section increased dramatically. Figure 6a shows the velocities at central crossings for three orbits with similar starting points in the three potentials defined by $m_0 = 10^{-1}, 10^{-2}$ and 10^{-3} , with $M_{BH} = 0$. In the potential with the smallest core, the orbit fills a large fraction of the surface of section during the period of integration; the only indication that the behavior is not fully random is a clustering of the points in two or three sub-regions of the octant. This nearly-random behavior on the surface of section was typical of most of the stochastic orbits in the potential with $m_0 = 10^{-3}$. A similar, though smaller, degree of scatter was produced by stochastic orbits in the $m_0 = 10^{-2}$ potential.

These results suggest that the degree of trapping of stochastic orbits – unlike the total *number* of stochastic orbits – depends strongly on the departure of the potential from integrability. Triaxial potentials with large cores are effectively integrable, not because the number of stochastic orbits is small, but because these orbits behave like regular orbits over astronomically interesting timescales. The high degree of trapping observed by Goodman & Schwarzschild (1981) was apparently due to their choice of a triaxial potential with a large core.

Increasing the black hole mass had a similar effect to decreasing m_0 . Figure 6b shows surfaces of section for three orbits in the potential with $m_0 = 0.1$, and $M_{BH} = 0.001, 0.003$ and 0.01 . Most of the stochastic orbits in the model with the smallest black hole act only slightly less trapped than in the corresponding model with $M_{BH} = 0$. However a larger M_{BH} produces more scatter, and when $M_{BH} = 0.01$, many of the stochastic orbits appear to scatter nearly randomly over the surface of section. Thus, either a small core ($m_0 \lesssim 10^{-2}$) or a massive central singularity ($M_{BH} \gtrsim 0.003$) causes the majority of the stochastic orbits to behave ergodically over astronomical timescales.

But even in the potentials with small m_0 and large M_{BH} , a certain fraction of the stochastic orbits were found to remain constrained to small areas on the surface of section. Among orbits from the same isoenergetic ensemble, we found that the amount of scatter on the surface of section correlated fairly well with σ_1 and σ_2 . Trapped stochastic orbits had Liapunov exponents that were smaller than average, usually lying between the two peaks in the histogram associated with the regular orbits and the stochastic orbits. We found that the separation was particularly clear in histograms of the “Kolmogorov entropy” $h_K = \sum_{i=1}^3 \sigma_i$, the sum of the three Liapunov exponents. (Since $\sigma_3 \approx 0$, h_K is essentially the sum of the two largest exponents.) For instance, when Liapunov exponents were computed over a time interval of $10^3 T_D$, most of the trapped stochastic orbits were found to have values of h_K that were less than ~ 0.5 times the maximum value for the ensemble. Figure 7 is a map of the starting points of trapped stochastic orbits defined in this way for two models: $m_0 = 10^{-3}$, $M_{BH} = 0$ and $m_0 = 10^{-1}$, $M_{BH} = 3 \times 10^{-3}$. The trapped orbits are not distributed randomly on these plots, but instead tend to cluster around the starting points of the regular orbits.

Since trapped orbits can mimic regular orbits for astronomically interesting timescales, they might be useful building blocks for real galaxies. Schwarzschild (1993), in a study of self-consistent models of galactic haloes, allowed each of the stochastic orbits to have its own weight – in effect assuming that every stochastic orbit was trapped. Merritt & Fridman (1996), in their “fully mixed” models, made the opposite assumption, i.e. that all stochastic orbits belong to invariant ensembles. The true situation lies between these extremes: trapped stochastic orbits can legitimately be treated like regular orbits, at least over appropriate timescales, but the remainder of the stochastic orbits at a given energy behave ergodically and should be assigned to ensembles with a fixed density distribution.

5. MIXING

5.1. Definitions

The Liapunov exponents, as well as the scatter on the surface of section, are measures of the time-averaged behavior of an orbit. But nature is less concerned with time averages than with the rate of evolution, at a given time, of ensembles. For instance, a regular orbit covers its invariant torus ergodically in a time-averaged sense, but an ensemble of points on the same torus does not evolve toward a steady state – it simply translates, unchanged, around the torus. Here we investigate the more interesting sort of relaxation that takes place when an ensemble of stochastic trajectories, initially confined to a small phase space region, evolves to fill (in a coarse-grained sense) the larger region accessible to it. This

process is similar to what occurs in a mixing system and we will use the term “mixing” to describe the evolution that we see. However we emphasize that a rigorous proof that mixing, as defined by mathematicians (Arnold & Avez 1968), takes place in our system would be extremely difficult. Our more modest goal is to show that the signatures of mixing behavior – erasure of correlations and evolution toward a coarse-grained steady state – are present and to estimate the timescale over which this evolution occurs.

We need first to define what we mean by a “fully-mixed” state, and then to define a measure of the distance between this state and the coarse-grained density of the evolving ensemble. The mixing rate will then be defined as the rate at which this distance measure approaches zero (e.g. Kandrup & Mahon 1994).

A stochastic trajectory of energy E moves within a five-dimensional phase space region. An obvious definition of the fully-mixed state would be a constant phase space density throughout this region. However it is not practical to keep track of the motion within a region of such high dimensionality, nor can we easily identify the regular and stochastic parts of phase space. Instead, we will base our analysis on the three-dimensional, configuration space density $\rho(\mathbf{x}, t)$ of the evolving ensemble. The coarse-grained equivalent of ρ will be specified via the occupation numbers n_i of particles within a set of Cartesian cells.

Since a stochastic trajectory will eventually visit every point in configuration space that lies within the equipotential surface, a simple measure of the departure from a fully-mixed state would be the fraction F of configuration space cells, lying beneath the equipotential surface, that contain no particles at a given time. $F = 0$ then corresponds to a fully-mixed state. This definition ignores the detailed number of particles within the cells; it indicates only the fraction of accessible volume that is occupied in a coarse-grained sense.

A better description of a fully-mixed state is the density corresponding to a uniform population of the energy surface $E = E_0$, or

$$\rho_{MC}(\mathbf{x}) \propto \int \delta(E - E_0) d^3v = C \sqrt{E_0 - \Phi(\mathbf{x})}, \quad \Phi(\mathbf{x}) \leq E_0. \quad (18)$$

This “micro-canonical” density is still only an approximation to the fully-mixed state, since no stochastic orbit can sample the full energy surface – regions corresponding to the regular orbits are excluded. However ρ_{MC} is easy to compute, and in a strongly stochastic system, we might expect ρ to approach ρ_{MC} fairly closely.

A third, and precise, definition of a fully-mixed state would be the density reached, after an infinite integration time, by an ensemble of particles that evolves according to the equations of motion in stochastic phase space. We can never compute this density exactly, but we may be able to approximate it in cases where the mixing is sufficiently rapid.

The “distance” between $\rho(\mathbf{x}, t)$ and $\rho_{MC}(\mathbf{x})$ can be defined in various ways. One way is in terms of the Jaynes entropy (Dejonghe 1987),

$$S(\rho, \rho_0) = - \int \rho \left[\ln \left(\frac{\rho}{\rho_0} \right) - 1 \right] d\mathbf{x} \quad (19)$$

with ρ defined as the probability density function in configuration space, normalized such that $\int \rho(\mathbf{x}, t) d\mathbf{x} = \int \rho_0 d\mathbf{x} = 1$. In discrete form, the corresponding distance measure $1 - S(\rho, \rho_0)$ becomes

$$D_1(n_i, n_{0i}) = \sum_i n_i \ln \left(\frac{n_i}{n_{0i}} \right), \quad (20)$$

where n_i is the number density of particles in configuration-space cell i , and n_{0i} is the number density of particles predicted by the reference density, or ρ_{MC} in the present case. The cell densities are normalized such that $\sum_i n_i = \sum_i n_{0i} = 1$. Equation (19) measures the logarithm of the probability that the n_i would have been measured if the occupation numbers were generated from the distribution n_0 . S is maximized, $S = 1$, when $n_i = n_{0i}$ for all i , and the fully-mixed state therefore has $D_1 = 0$. In the limit $n_i \rightarrow n_{0i}$, we have $\ln(n_i/n_{0i}) \rightarrow \ln(1 + \delta) \rightarrow \delta$ where $\delta = (n_i - n_{0i})/n_{0i}$. Thus

$$D_1 \rightarrow \sum_i n_i \left[\frac{n_i}{n_{0i}} - 1 \right]. \quad (21)$$

Another measure of the approach of the density distribution to the fully-mixed state is the mean square difference in the cell occupation numbers, or

$$D_2(n_i, n_{0i}) = \sum_i \left[\frac{n_i - n_{0i}}{n_{0i}} \right]^2 n_{0i} \quad (22)$$

$$= \sum_i n_i \left[\frac{n_i}{n_{0i}} - 1 \right]. \quad (23)$$

Similar measures of distance were adopted by Mahon *et al.* (1995) and by Merritt & Fridman (1996). This distance measure is equivalent to the entropy-based measure D_1 when $n_i \approx n_{0i}$. Once again, $D_2 = 0$ in the fully mixed state.

We found that D_1 and D_2 behaved in similar ways with time but that D_2 was more noisy; hence we present plots only of D_1 below.

In a real galaxy as in our ensembles, the total number of stars is finite. Consequently, even in a fully-mixed state, an arbitrarily selected volume of phase space (or configuration space) may not contain a single star even if the probability of finding a star in that volume is high. This provides us with a physical constraint on the degree of coarse graining to

apply. Too coarse a mesh would show little evolution after early times and too fine a mesh would show large fluctuations even at late times. We defined our mesh as a $10 \times 10 \times 10$ cubic grid with edge length slightly greater than the amplitude of the axial orbit. We found from experimenting with larger and smaller meshes that the errors arising from large fluctuations in cell occupancy were generally lower for this mesh. When computing ρ_{MC} , densities lower than that corresponding to one particle in a grid cell were assigned the value zero to avoid comparing the cell densities at the outer edges of the distribution with infinitesmally small values.

5.2. Approach to a Fully-Mixed State

We evolved a number of isoenergetic ensembles of 10^4 particles in two of our model potentials: $m_0 = 10^{-3}$, $M_{BH} = 0$ (hereafter Model 1), and $m_0 = 10^{-1}$, $M_{BH} = 3 \times 10^{-3}$ (Model 2). The starting points of the particles in each ensemble were chosen randomly from a small patch on the equipotential surface, surrounding one of the points on the regular grid of initial conditions, as shown in Fig. 7. All ensembles had an energy equal to that of the x -axis orbit that just touches the ellipsoidal shell dividing the model into two equal-mass parts. Each patch was approximately square and had an edge length roughly equal to the separation between grid points. Two of the ensembles from each model were centered about the starting points for trapped stochastic orbit, while the remainder were centered about non-trapped stochastic orbits. The evolution time was $200T_D$ for all ensembles – an interval that is comparable to the dynamical age of most of the stars in a bright elliptical galaxy.

We chose the starting points to lie on the equipotential surface because only then could we be reasonably certain that most of orbits in an ensemble were stochastic. However it is still possible that some of the particles in each ensemble lay close to a stable, high-order resonance and thus were regular.

The evolution of one ensemble, No. 2 from Model 1, is illustrated in Figure 8. The starting points for this ensemble surround a strongly stochastic orbit and the mixing takes place very rapidly. After 15 dynamical times (roughly 5 Liapunov times) the clump has evolved into a filament containing several knots, although some particles have broken free of the filament. After about 30 dynamical times, the ensemble appears to have filled most of the volume beneath the equipotential surface, though in a highly nonuniform way. By about 75 dynamical times, the ensemble appears to be approaching a time-invariant density distribution. Most of the particles in this near-invariant distribution fill a region similar in shape to that of a regular box orbit.

The distribution of points at the final time step, $T = 200T_D$, is shown in Figure 9 for two ensembles. The distributions appear to be nearly symmetric and unevolving at this late time; the snapshots of Figure 9 have accordingly been symmetrized about the principal planes to improve the statistics. The density is highest in both cases near the x axis and lowest near the z axis – in other words, the distribution has the same approximate shape as the model density.

The density distributions of Figure 9 represent nearly unchanging populations of chaotic phase space. As such, they constitute bona fide building blocks for galaxies. We assume that nature would make use of these invariant densities in much the same way that it makes use of regular orbits.

The rate at which the different ensembles fill the volume within the equipotential surface, as measured by our parameter F , is shown in Figure 10. We see that the non-trapped ensembles evolve to fill most or all of this volume after only a few tens of crossing times, i.e. of order ten Liapunov times. The filling rate is highest for ensembles whose starting points lie near the z -axis or near the $y - z$ plane – the part of initial-condition space which corresponds to the highest Liapunov exponents. The trapped orbits, on the other hand, fill only a fraction of the accessible volume even after 200 dynamical times. The value of F oscillates strongly for these trapped ensembles as the phase points slosh coherently from one side of the potential to the other – the near-quasi-periodicity of the trajectories causes them to remain correlated for a long time. (We carried out some additional experiments with ensembles in regular phase space. They maintained their coherence even longer than the trapped stochastic ensembles, mixing almost not at all during the 200 dynamical times.) We note also that there is a continuity in mixing behaviors between the “trapped” and “non-trapped” ensembles. For instance, ensemble No. 2 from Model 1 (non-trapped) evolves about as quickly as ensemble No. 6 (trapped).

A better measure of the departure from a fully-mixed state is shown in Figure 11, which plots $D_1(n_i, n_{MCi})$, the distance from the micro-canonical density, as a function of time. These curves are very similar to those presented by Kandrup & Mahon (1994) in their study of mixing in a two-dimensional, truncated Toda lattice, and many of the points made by them apply to our results as well. The decay of D_1 is initially roughly exponential; the convergence rate $|d \ln D_1/dt|$ is approximately $0.03 - 0.1T_D^{-1}$ for the non-trapped ensembles in both models, but rather longer (and not so clearly exponential) for the trapped ensembles. This decay eventually slows, at which point D_1 for the non-trapped ensembles is fairly small, $0.2 < D_1 < 0.5$, corresponding to a nearly-uniform filling of the energy surface. Of course a nonzero, asymptotic value for D_1 is expected since the fully-mixed density is different from the micro-canonical density. However the fact that different ensembles tend

to significantly different values of D_1 over these timescales indicates that the slow-down in the evolution of D_1 is due to a real decrease in the rate of mixing.

5.3. Effect of Noise on the Mixing Rate

Smooth, symmetric potentials are idealized representations of real galaxies, which often exhibit deviations from ellipsoidal symmetry, imbedded disks, or other fine structure. As seen by a single star, these distortions would add small-amplitude perturbing forces to the smooth forces produced by the overall mass distribution. There may be other sources of time-dependent forces as well, including close encounters with stars in the dense central cusp, tides from satellite galaxies, etc. During galaxy formation such perturbations would be very large, and slow oscillations in the potential might persist thereafter for many dynamical times as a galaxy evolves toward a steady state.

These weak or slow perturbations would not be expected to have a big effect on either the regular, or the strongly stochastic, orbits. The former would preserve their adiabatic invariants, while the latter move nearly randomly through phase space whether or not they are perturbed. But small perturbations might have an appreciable effect on the mixing rate of weakly stochastic or trapped orbits, since the perturbations could carry stars away from a trapped region into a more strongly stochastic region. Goodman & Schwarzschild (1981) found that perturbations had relatively little effect on the behavior of orbits in their Hubble-law potential; however Habib, Kandrup & Mahon (1995), in a study of motion in a two-dimensional potential, found that even small amounts of noise could greatly enhance the mixing.

Following Goodman & Schwarzschild (1981), we introduced noise into our mixing calculations by adding random impulses that changed the instantaneous direction of the velocity vector of a particle at regular intervals. All of the particles in the ensemble were perturbed together, although no two particles received the same perturbation. This scheme left the energies of the particles unchanged. Habib, Kandrup & Mahon (1995) employed a more sophisticated prescription for adding noise but their scheme was also designed to preserve energy; thus our results might be roughly comparable to theirs.

The average rate of change of the transverse velocity due to perturbations is

$$\delta_t v_{\perp}^2 = Dv_{\perp}^2/Dt. \quad (24)$$

A physically interesting number with which to compare this is the standard diffusion

coefficient for star-star encounters,

$$\langle(\Delta v_{\perp})^2\rangle = 8\pi G^2 m_f^2 n_f \frac{3 \ln(0.4N)}{2 v_{mf}} \times 0.583, \quad (25)$$

(Spitzer & Hart 1971), where v_{mf} , the rms velocity of the field stars, has been assumed to be equal to that of the test star. We can estimate $\langle(\Delta v_{\perp})^2\rangle$ for our models by assuming that the total number of stars in the system is 10^{11} each with a mass of $1\mathcal{M}_{\odot}$, and identifying n_f with $\bar{\rho}/m_f$, where $\bar{\rho}$ is the mean density within the half-mass radius. The mean velocity of the field stars is taken to be $v_{mf} = 4X_0/T_0$ where X_0 and T_0 are the amplitude and period of the x -axial orbit with the same energy as that of our ensembles. We find $\langle(\Delta v_{\perp})^2\rangle \approx 2 \times 10^{-9}$ in model units, corresponding to a relaxation time of $\sim 10^7 T_D$.

We then define the strength of the imposed perturbations via the parameter η , where

$$\eta = \delta_t v_{\perp}^2 / \langle(\Delta v_{\perp})^2\rangle. \quad (26)$$

We chose η to have one of the three values $1, 10^2$ or 10^4 , similar to the choices made by Goodman & Schwarzschild (1981). The last choice is clearly an overestimate of the perturbation size to be expected from star-star encounters, but it is still quite modest when interpreted as a representation of perturbations from other possible sources. The two-body relaxation time as we have defined it is of order 10^7 dynamical times in our models, so a value of $\eta = 10^4$ corresponds to a perturbation timescale of $1000T_D$ – quite a weak perturbation.

While in principle the time interval between successive perturbations should be described by a Poisson distribution and the amplitude of the individual perturbations should be random, we have assumed for simplicity of programming that the perturbations occur at regular intervals and are of equal amplitude. Having specified η , one still has the freedom to specify how often the perturbations are applied. We followed the example of Goodman & Schwarzschild (1981) by perturbing the particles roughly once per dynamical time.

The results are shown in Figure 12, for $\eta = 10^4$; smaller amplitude perturbations were found not to significantly affect the mixing rate of any ensemble. We find that noise with this amplitude is quite effective at accelerating the mixing. All of the ensembles now evolve in a similar way, and at late times, every ensemble appears to be approaching a common final state. Furthermore, the distinction between trapped and non-trapped ensembles is much reduced in the presence of noise. It seems reasonable to conclude that random perturbations can significantly enhance the mixing rates of ensembles of stochastic orbits, causing even ensembles of trapped orbits to reach an invariant distribution in perhaps a few hundred orbital times.

5.4. Mixing Timescales

We see in Figures 11 and 12 evidence of two timescales associated with the mixing. The mixing is initially fast, with a roughly exponential dependence of D_1 on time. Subsequent mixing is slower and continues until the end of the integrations at $t = 200T_D$. These two regimes are evident in all of the integrations that included noise. In the absence of noise, the non-trapped ensembles evolve in this way but the evolution of the trapped ensembles is more complex.

The existence of a second, longer timescale for the orbital evolution was noted above in the discussion of the Liapunov exponents. It is reasonable to suppose that the slower mixing seen in Figures 11 and 12 takes place on roughly the same timescale over which the Liapunov exponents were observed to evolve toward a common value in §3 – i.e. hundreds or thousands of orbital times. After elapsed times of this order (or perhaps less in the integrations including noise) we would expect all of the stochastic ensembles to have attained very nearly the same density distribution. Limited computing resources kept us from verifying this prediction.

Kandrup and coworkers (Kandrup & Mahon 1994; Mahon et al. 1995; Habib, Kandrup & Mahon 1995) also noted the existence of a long and a short timescale associated with mixing in their two-dimensional potentials. Kandrup & Mahon (1994) found the initial mixing rate to be roughly 0.15 times the rate of divergence of nearby trajectories in their truncated, Toda-lattice potential. The initial rate of decay of D_1 in our non-trapped ensembles is difficult to estimate with any accuracy. At first the decay is very rapid, and appears to take place at a rate that is approximately equal to the inverse Liapunov time. The decay rate continually slows, however, and an average rate over the first 50 orbital times is of order $0.03 - 0.1T_D^{-1}$ in the absence of noise, compared to a typical Liapunov exponent of $0.3T_D^{-1}$. The corresponding ratio is $\sim 0.1 - 0.3$, in good agreement with Kandrup & Mahon’s result. This agreement is not surprising: it simply reflects the fact that the mixing is driven initially by the orbital instability and so its characteristic time is tied to the Liapunov time. We assume that mixing would continue at this rate except for the existence of barriers in phase space, i.e. invariant tori and “cantori” that inhibit the diffusion (Mackay, Meiss & Percival 1984).

We note that certain features of the $D_1(t)$ curves are dependent on the details of our numerical treatment. If our initial conditions had been selected from smaller patches on the equipotential surface, or if we had used a finer grid to compute D_1 , we would have observed a longer exponential decay, because more time would have been required for the mixing to eliminate correlations on the scale of the grid cells. Stated differently, the coarse-grained relaxation time depends on the level of coarse-graining.

However, the rate $|d \ln D_1/dt| \equiv T_M^{-1}$ at which correlations initially decay should not be a strong function of these details. Kandrup & Mahon (1994) found this to be the case, as did we, based on a limited number of additional experiments with different numbers of grid cells.

We did not investigate the dependence of the mixing rate on energy. However Kandrup & Mahon (1994) found a fairly constant ratio between the Liapunov and mixing timescales at different energies in their two-dimensional potentials, and the same may be true in our models. Merritt & Fridman’s (1996) results (their Figure 8b) suggest that this is approximately true.

Which of these two timescales should we associate with the mixing in real galaxies? The answer is probably: both. The initial, exponential decay of D_1 reflects the erasure of correlations due to the instability of the motion; after several of these decay times have elapsed, the ensemble has filled, in a coarse-grained sense, most of the configuration-space region accessible to it. Inspection of Figure 8 and other plots like it suggests that a time of $\sim 100T_D$, i.e. $\sim 5T_M$, can be roughly identified with this “relaxation time.” This is an astronomically interesting timescale; orbital periods at the half-light radii of bright elliptical galaxies are of order 10^{-2} times the age of the universe (§6).

The slower mixing that is associated with diffusion into the Arnold web might cause a galaxy to continue to evolve in shape as the stochastic orbits mix toward their invariant distributions. We were not able to estimate this longer timescale with any precision, but there are a number of indications that it is of order 10^3T_D . Such a number is consistent with the slow decay seen on Figures 11 and 12, and with rate of approach of the Liapunov exponents toward a common value in Figures 3-5. Merritt & Fridman (1996) also found that the time required for single stochastic orbits to behave “ergodically” was of order 10^3T_D .

These timescales might be substantial overestimates if galaxies are efficiently mixed during their formation. This possibility is discussed further below.

In potentials with larger cores or smaller central singularities, we showed above that a larger fraction of the stochastic orbits mimic regular orbits for hundreds or thousands of oscillations. We expect mixing to be less efficient in these models, with the mixing rate approaching zero as $m_0 \rightarrow 1$ or $M_{BH} \rightarrow 0$. It follows that galaxies might differ enormously in the degree to which their stochastic orbits are mixed, a point that we return to in §6.

6. Discussion

We discuss three issues raised by this work: the applicability of Jeans’s theorem to systems containing stochastic orbits; the relation between chaotic mixing and violent relaxation; and the importance of chaos for the structure and slow evolution of elliptical galaxies.

6.1. Jeans’s Theorem

Jeans’s theorem specifies the conditions under which a collisionless stellar system will be in a state of equilibrium. In modern texts (as well as in Jeans’s original formulation) the theorem is usually restricted to systems that are fully integrable, i.e. in which all or virtually all of the orbits respect a number of isolating integrals equal to or greater than the number of degrees of freedom. Binney & Tremaine (1987) call this restricted version the “strong Jeans theorem” and base its derivation on the time-averages theorem, i.e. the ergodic property of regular orbits. Binney (1982b) argues further that the lack of a general proof of ergodicity for irregular orbits calls into question the applicability of Jeans’s theorem to more general, non-integrable systems.

We do not see a clear link between ergodicity – which is a time-averaged property of trajectories – and stationarity, which is a statement about conditions at a single time. We would accordingly state the requirements for a stationary state in a different way, even in systems that are fully regular. Suppose one divides the phase space of a system with a fixed potential into a set of regions, each of which is filled by a single orbit. For regular orbits, these regions are invariant tori, while for irregular orbits the regions are more complex in shape. A sufficient condition for a steady state is that the phase-space density f be constant within each of these regions. The proof follows directly from Liouville’s theorem: since f is conserved following the flow, an initially constant value within any bounded region will remain constant forever. This proof relies purely on the incompressibility of the flow; no additional properties of the motion – such as ergodicity or mixing – are required.³ We therefore disagree with derivations of Jeans’s theorem that imply a link between stationarity and ergodicity.

³Just this point of view is implicitly taken by anyone who writes $f = f(E, L_z)$ for an axisymmetric galaxy. Such a distribution function assigns nonzero densities to stochastic parts of phase space, in general, and yet it describes a steady state since f is forced to be constant throughout any chaotic subregions of the hypersurfaces defined by constant E and L_z . The ergodicity of the motion in those stochastic regions is of no importance.

The situation is not quite this simple, however, since collisionless stellar systems have no built-in mechanism by which the fine-grained distribution function can evolve to such a state. The importance of properties like ergodicity or mixing – which are effectively measures of the degree of randomness of the flow (Lichtenberg & Lieberman 1983, p. 273) – are that they can sometimes guarantee the approach to a coarse-grained steady state. The way this works in the case of a purely regular system was discussed in §1, and the evolution of chaotic flows toward near-invariant distributions was the subject of §5. Thus, while the possibility of stationary configurations depends only on Liouville’s theorem, which is valid generally, relaxation toward a coarse-grained steady state will only occur if the flow satisfies more stringent conditions.

Another relevant point is the difficulty of dividing phase space into “chaotic” and “regular” regions. The Arnold web is believed to permeate the entire phase space, intersecting or lying infinitesimally close to every point, even points associated with regular orbits (Lichtenberg & Lieberman 1983, p. 54). It would therefore be extremely difficult in practice to define what is meant by the “chaotic part of phase space” at a given energy. However one could imagine approximating a uniformly-filled, chaotic phase space by evolving an ensemble of points until their coarse-grained density was nearly unchanging, as was done here in §5. The required evolution time might be extremely long, although the addition of noise to the forces might accelerate the mixing. Such a scheme would allow one to incorporate the chaotic parts of phase space into time-independent models. Nature presumably does something very much like this when it makes real galaxies.

6.2. Violent Relaxation

In a real galaxy, however, the approach to a stationary state takes place against the background of a time-varying potential. Following Lynden-Bell’s (1967) pioneering paper, potential fluctuations have generally been credited with producing the relaxation. Lynden-Bell identified the collisionless relaxation time as

$$T_r = \frac{3}{4} \langle \frac{\dot{\Phi}^2}{\Phi^2} \rangle^{-1/2}, \quad (27)$$

with $\dot{\Phi}$ the rate of change of the gravitational potential, and argued that “violent relaxation” should take place on roughly this timescale.

It is clear that a rearrangement of stars in energy space can only take place if the gravitational potential is time-dependent. But it is less clear that there exists a deeper link between potential fluctuations and collisionless relaxation. Our experiments (and those

of Kandrup and co-workers) demonstrate that a time-varying potential is not necessary for strong evolution of the phase-space distribution to take place: mixing toward a steady state can occur in a completely fixed potential. (Phase mixing is of course another example of such evolution, as pointed out by Lynden-Bell.) Nor is relaxation guaranteed to occur simply because the potential is fluctuating. Consider for example a group of stars that sit motionless at the center of a collapsing proto-galaxy. The energy of these stars changes as the galaxy collapses, but no relaxation of any physically interesting sort takes place: the stars remain fixed in phase space as their energies change. More generally, one can imagine enclosing a stellar system inside a massive spherical shell whose radius is varied with time. The potential within the galaxy will fluctuate, but there are no forces from the shell and hence no relaxation.⁴ Changes in the potential imply here only a relabeling of the particle energies; they do not, by themselves, constitute relaxation.

A time-varying potential can even *inhibit* evolution. For instance, the stars in a dense satellite that spirals into a larger galaxy are slow to mix, because the self-gravity of the satellite maintains the coherence of their motion. If this self-gravity were turned off, allowing the stars to move in the *fixed* potential of the larger galaxy, they would be free to phase-mix. Thus the time-varying component of the potential acts in this case to maintain correlations, not to destroy them.

It seems evident that relaxation – by which we mean “evolution to a stationary state” – in collisionless stellar systems always requires a divergence in particle trajectories, that is to say mixing, since only through mixing can memory of the initial conditions be erased. Potential fluctuations constitute relaxation only to the extent that they promote mixing. Many of the specific physical mechanisms that are thought to cause collisionless relaxation during galaxy formation can be usefully thought about in this way. For instance, in “potential scattering,” a star gains energy by falling in through a deep potential well and escaping through a shallow one. But this energy gain is of no importance by itself; it leads to relaxation only if nearby stars gain different amounts of energy, since otherwise those stars will remain in fixed positions relative to one another. In other words, potential scattering contributes to relaxation only insofar as it causes initially nearby particles to move apart. But it is the divergence in phase space, and not the energy change per se, that is correctly identified with the relaxation.

If the potential fluctuations are sufficiently rapid or strong, we might guess that chaotic mixing – or something like it – will take place in no more than a collapse or crossing time, as in Lynden-Bell’s picture. The rapid approach to equilibrium seen in *N*-body

⁴We thank R. Miller for suggesting this example.

experiments suggests that this is approximately the case. However it is still the mixing process, and not the potential fluctuations themselves, that is responsible for the relaxation. The chaotic mixing experiments described here in a fixed potential might therefore provide a simple picture of the way in which collisionless relaxation takes place under more general conditions.

6.3. Importance of Chaotic Mixing for the Structure and Evolution of Elliptical Galaxies

Schwarzchild (1993) and Merritt & Fridman (1996) argue that many or most of the stars in triaxial stellar systems could be on stochastic orbits. If so, elliptical galaxies might evolve on timescales that are similar to the timescales for chaotic mixing derived here.

One problem with this simple view is the difficulty of comparing the mixing rates in the regular and stochastic parts of phase space. It is often loosely stated that regular orbits fill their tori in a short time – some small multiple of an orbital period – while stochastic orbits diffuse more slowly. According to this view, any slow evolution would be driven purely by the diffusion of the stochastic orbits. But such statements confuse ergodicity with mixing. While the *time averaged* density of stars on an invariant torus approaches a coarse-grained steady state in a few crossing times, an *ensemble* of stars on a regular orbit never relaxes. One could take the extreme view that mixing of stochastic orbits is infinitely faster than that of regular orbits, since a collection of stars confined to a single regular orbit does not mix!

In fact it seems likely that the evolution to a near-stationary state takes place mostly during galaxy formation, when the potential is strongly time-dependent and the motion is essentially chaotic. Once the potential begins to settle down, some stars will find themselves in regular parts of phase space and some in stochastic parts; in regions of both types, the phase space distribution will be highly mixed and, perhaps, not far from a coarse-grained steady state. Subsequent evolution would be driven both by phase mixing and by chaotic mixing. We do not know which of these two types of mixing would dominate the evolution in a typical case; perhaps both would be important.

However, the consequences of continued mixing would be very different for the two types of orbit. A non-mixed region of regular phase space – a non-uniformly populated torus, for example – would almost always generate a lopsided configuration-space density (Eq. 2). But an ensemble of stochastic orbits can be symmetric in configuration space even if it does not fully populate its allowed phase space region. In fact ensembles of trapped

stochastic orbits appear to evolve in much this way, quickly reaching a nearly symmetric shape before more slowly diffusing into the full Arnold web. Real elliptical galaxies often – though not always – appear to have a high degree of symmetry, which suggests that their regular parts of phase space are nearly fully mixed.

There is a second way in which the consequences of phase mixing and chaotic mixing are different. Mixing in stochastic phase space leads to a reduction in the effective number of orbits, since it replaces all the stochastic trajectories at a given energy by a single invariant density distribution. If chaotic mixing timescales are short compared to a galaxy lifetime, this reduction might force a galaxy to evolve away from a triaxial shape toward an axisymmetric one (Schwarzschild 1981). On the other hand, if chaotic mixing timescales are long, then elliptical galaxies might persist in slowly evolving, approximately triaxial shapes. Which of these two descriptions is most correct depends only on the ratio of the chaotic mixing timescale to the galaxy lifetime (and, of course, on the fraction of stars that follow chaotic trajectories).

The results presented here and by other workers suggest that this ratio is strongly dependent on the central structure of a galaxy. In a triaxial model with a low central concentration of mass, many of the boxlike orbits may be stochastic, but these stochastic orbits behave very much like regular orbits for hundreds or thousands of crossing times. Goodman & Schwarzschild (1981) first described such behavior in their study of a triaxial model with a Hubble-law profile, and we observed similar behavior for the orbits in our models with large m_0 and small M_{BH} . Models with cores do not describe early-type galaxies very well. However Merritt & Fridman (1996) found that the stochastic motion in triaxial models with shallow cusps, $\rho \propto r^{-1}$, was similar to that seen here in models with cores. This is reasonable since the gravitational force generated by a weak power-law cusp is finite near the center.

On the other hand, a steep central cusp or a massive central singularity can persuade most of the stochastic orbits to behave ergodically over much shorter timescales. Precisely how steep a cusp is required is not yet known. The models studied here have a fixed central slope, $\rho \propto r^{-2}$, for small m_0 – the same central dependence as in Schwarzschild's (1993) scale-free models and in Merritt & Fridman's (1996) “strong cusp” model. Presumably the transition from effectively regular behavior to effectively ergodic behavior for the majority of stochastic orbits takes place somewhere between $\rho \propto r^{-1}$ and $\rho \propto r^{-2}$; one would like to know exactly where. In the case of central singularities, the results of §4 suggest that the critical mass for inducing ergodic behavior is about 0.3% of the galaxy mass.

The strong dependence of the orbital behavior on the degree of central mass concentration suggests that triaxial galaxies might come in two distinct families: those

in which the orbital motion is nearly regular, and those in which the stochastic parts of phase space are nearly mixed. The latter galaxies might not persist for long in triaxial configurations due to the limited number of orbital shapes that would be available for maintaining a non-axisymmetric shape.

One consequence is that faint elliptical galaxies are less likely to be triaxial than bright ones. Ellipticals with absolute luminosities less than $M_B \approx -20$ have the steepest central density cusps on average, with logarithmic slopes γ in the range $-2 \lesssim \gamma \lesssim -1$, compared to $0 \lesssim \gamma \lesssim -1$ for brighter ellipticals (Gebhardt et al. 1996). Low-luminosity ellipticals also have higher average densities, and shorter dynamical times, than bright ellipticals; all else being equal, the mixing will have gone farther in these galaxies.

For an estimate of the dynamical ages of bright ellipticals, we refer to Katz & Richstone's (1985) study of three galaxies, NGC 4472 ($M_B = -22.1$), 4374 (-21.1), and 4636 (-20.9). Adopting their inferred M/L of 19.5 in solar units ($H_0 = 75$), we find for the circular orbital period at the effective radius 1.3×10^7 , 4.3×10^7 and 1.86×10^7 yr, respectively. Assuming a galaxy lifetime T of 5×10^9 yr, the “dynamical ages” T/T_D of these bright galaxies are 38, 115 and 27 at the half-light radius. We estimated above (§5) that relaxation to a strongly mixed state might require of order $10^2 T_D$ in a triaxial galaxy with a strong central concentration of mass. Thus – even assuming that these bright ellipticals have massive nuclear black holes – we would expect them to be strongly mixed only in their central regions, $r \lesssim r_e$.

For comparison, we computed dynamical ages of several low-luminosity ellipticals ($M_B \approx -19$) with known distances, assuming the same M/L as above. Typical half-mass orbital times were found to be 4×10^7 yr, with dynamical ages in the range 100 – 200. The combination of larger dynamical ages with steeper central cusps implies that the stochastic orbits in low-luminosity, triaxial ellipticals would be more strongly mixed than in bright ellipticals.

(Bright ellipticals are also more likely to have undergone a recent merger event, and in this sense too might be dynamically “younger” than faint ellipticals.)

An extreme example is the nearby dwarf elliptical M32, which is known to have a steep central density cusp, $\rho \propto r^{-1.63}$ (Gebhardt et al. 1996), as well as a central mass concentration containing $\sim 0.3\%$ of the stellar mass (Tonry 1987). M32 is also atypically dense: the circular orbital time at the half-light radius is only about 10^7 yr (Dehnen 1996), implying that most of the stars in M32 have completed 10^3 orbits or more since the galaxy formed. Triaxiality would presumably be difficult to maintain in this galaxy, and in fact detailed modelling (Dehnen 1995; van der Marel et al 1994) suggests that M32 is nearly

oblate.

There are two complications to this simple picture. First, it is possible that most or all early-type galaxies contain massive central singularities (Kormendy & Richstone 1995). If so, the steepness of the stellar cusp would be of secondary importance for determining the degree of stochasticity – because the motion of the boxlike orbits would be strongly chaotic even in the absence of a cusp. Second, faint elliptical galaxies are often rapidly rotating (Davies et al. 1983). The effect of figure rotation on the degree of stochasticity in triaxial models has not yet been well explored.

Leaving aside for the moment these complications, we can ask whether there is any evidence that bright elliptical galaxies have systematically different shapes than faint ellipticals. There is in fact an emerging consensus for such a dichotomy (e.g. Kormendy & Bender 1996): low-luminosity ellipticals are said to be “disky” and oblate, while high-luminosity ellipticals are “boxy” and triaxial.

The separation of elliptical galaxies into boxy and disk subgroups seems well established, but in our view the evidence that faint ellipticals are oblate while bright ellipticals are triaxial is not yet compelling. The most convincing test for triaxiality is minor-axis rotation. Franx, Illingworth & de Zeeuw (1991) found that relatively few galaxies exhibit kinematic misalignments – only about 8 galaxies in their sample of 38. However only one of their galaxies was fainter than $M_B = -20$, and there is no obvious tendency in their sample for the degree of kinematic misalignment to correlate with luminosity. Thus, little appears to be known at the present time about the relative frequency of minor-axis rotation in bright and faint ellipticals.

Tremblay & Merritt (1996) found that the distribution of Hubble types for bright ellipticals ($M_B \lesssim -20$) was significantly different than for faint ellipticals: bright galaxies appear rounder on average, and they have a distribution of apparent shapes that is difficult to reproduce under the axisymmetric hypothesis. However the Hubble-type data are equally consistent with triaxial shapes for both bright and faint galaxies.

Detailed modelling of individual elliptical galaxies has only begun; the example of M32, which is faint and apparently oblate, was discussed above.

We conclude that the observational data are consistent with a picture in which bright ellipticals are triaxial and faint ones oblate, but that such a picture is not yet compelling.

Within individual galaxies, the dynamical age is a function of radius, and we would sometimes expect the central regions of a triaxial galaxy to be highly mixed while the outer regions are still in the process of mixing. The transition between the two regions would

occur at the “mixing radius” R_M where the mixing time is equal to the age of the galaxy. Although it is difficult to calculate R_M with any precision, we can obtain a crude estimate by equating the galaxy lifetime to the time $\sim 100T_D$ that was found above to characterize mixing in strongly stochastic potentials. We find $R_M \lesssim r_e$ in the three bright galaxies discussed above and $R_M \gtrsim r_e$ in the fainter ellipticals; while in M32 this radius would lie well outside of r_e – this galaxy should be strongly mixed throughout. Even at radii less than R_M , mixing would be expected to continue at the slower rate seen in the experiments of §5.

Mixing near the center of a triaxial galaxy would tend to make the galaxy axisymmetric there. Observed from a random angle, such a galaxy would probably exhibit a non-constant ellipticity, and a major-axis position angle that varied with radius. Could this be the origin of isophote twists?

We were motivated to think about the issues discussed here in part by J. Binney’s provocative paper on the applicability of Jeans’s theorem to nonintegrable systems. Discussions with him, and also with O. Gerhard, D. Heggie, H. Kandrup, J. Laskar, R. Miller, T. Padmanabhan, D. Pfenniger and S. Tremaine helped to sharpen our thinking. W. Dehnen read the manuscript especially carefully and made a number of comments that led to improvements in the presentation. The computer programs used in this study for integrating orbits and computing Liapunov exponents were written by the Geneva group and graciously lent to us by S. Udry and D. Pfenniger. B. Tremblay supplied some of the numbers in §6. This work was supported by NSF grant AST 90-16515 and by NASA grant NAG 5-2803 to DM.

Table 1: Liapunov Exponents

M_{BH}	m_0	$\sigma_1 T_D$	$\sigma_2 T_D$	N
0	10^{-1}	0.14 ± 0.06	0.045 ± 0.02	85
	10^{-2}	0.21 ± 0.09	0.078 ± 0.03	141
	10^{-3}	0.27 ± 0.05	0.085 ± 0.02	152
10^{-3}	10^{-1}	0.15 ± 0.03	0.066 ± 0.02	163
	10^{-3}	0.27 ± 0.06	0.080 ± 0.02	151
3×10^{-3}	10^{-1}	0.20 ± 0.04	0.097 ± 0.02	159
	10^{-3}	0.28 ± 0.07	0.086 ± 0.02	152
10^{-2}	10^{-1}	0.28 ± 0.08	0.16 ± 0.04	171
	10^{-3}	0.32 ± 0.10	0.13 ± 0.04	163

A. APPENDIX

Computation of the Gravitational Forces

Here we present expressions for the gravitational forces corresponding to the triaxial mass models described in §2, and their derivatives, which are required when computing the Liapunov exponents. We also discuss the numerical techniques used to evaluate the forces quickly and accurately.

The forces may be derived from the potential gradient by computing the contributions to the force separately from the two different ellipsoidal coordinate systems. Thus if the potential is expressed as $\Phi(\mathbf{x}) = \Phi^{\mathbf{A}}(\mathbf{x}) + \Phi^{\mathbf{B}}(\mathbf{x})$, then the forces are $\mathbf{F}(\mathbf{x}) = \mathbf{F}^{\mathbf{A}}(\mathbf{x}) + \mathbf{F}^{\mathbf{B}}(\mathbf{x})$, with

$$\mathbf{F}^{\mathbf{A}}_x = -\frac{\partial \Phi^{\mathbf{A}}}{\partial x}, \quad (A1)$$

$$\mathbf{F}^{\mathbf{B}}_x = -\frac{\partial \Phi^{\mathbf{B}}}{\partial x}. \quad (A2)$$

The required gradients can be evaluated by using

$$\frac{\partial}{\partial x} = 2x \left[\frac{(\lambda - b^2)(\lambda - c^2)\partial}{(\lambda - \mu)(\lambda - \nu)\partial\lambda} + \frac{(\mu - b^2)(\mu - c^2)\partial}{(\mu - \nu)(\mu - \lambda)\partial\mu} + \frac{(\nu - b^2)(\nu - c^2)\partial}{(\nu - \lambda)(\nu - \mu)\partial\nu} \right]. \quad (A3)$$

The derivatives with respect to the cartesian coordinates y, z are similarly obtained by the substitutions

$$\lambda \rightarrow \mu \rightarrow \nu \rightarrow \lambda, \quad x \rightarrow y \rightarrow z, \quad a \rightarrow b \rightarrow c \rightarrow a.$$

It can be shown that

$$\frac{\partial G(\tau)}{\partial \tau} = \frac{2}{3} R_J(a^2, b^2, c^2, \tau), \quad (A4)$$

where $R_J(a^2, b^2, c^2, \tau)$ is Carlson's symmetrized version of the incomplete elliptic integral of the third kind which can be numerically evaluated by fast algorithms.

The forces are then given by

$$\mathbf{F}_x^A = \frac{2x}{3\pi(1-m_0)} [Q_{\lambda}^A R_J(a^2, b^2, c^2, \lambda) + Q_{\mu}^A R_J(a^2, b^2, c^2, \mu) + Q_{\nu}^A R_J(a^2, b^2, c^2, \nu)] \quad (A5)$$

$$\begin{aligned} \mathbf{F}_x^B = & \frac{-2x}{3\pi(1-m_0)m_0^2} [Q_{\lambda'}^B R_J(a^2, b^2, c^2, \lambda'/m_0^2) + Q_{\mu'}^B R_J(a^2, b^2, c^2, \mu'/m_0^2) \\ & + Q_{\nu'}^B R_J(a^2, b^2, c^2, \nu'/m_0^2)] \end{aligned} \quad (A6)$$

where we have adopted the shorthand notation

$$\begin{aligned} Q_\tau^A &= \frac{(\tau - b^2)(\tau - c^2)}{(\tau - \tau_+)(\tau - \tau_-)}, \\ S_\tau^A &= \frac{(\tau - c^2)(\tau - a^2)}{(\tau - \tau_+)(\tau - \tau_-)}, \\ T_\tau^A &= \frac{(\tau - a^2)(\tau - b^2)}{(\tau - \tau_+)(\tau - \tau_-)}, \end{aligned} \quad (\text{A7})$$

where since

$$\lambda \rightarrow \mu \rightarrow \nu \rightarrow \lambda$$

$\tau \equiv \lambda$ implies $\tau_+ \equiv \mu$ and $\tau_- \equiv \nu$ and likewise for the second set of coordinates (λ', μ', ν') with a^2, b^2, c^2 replaced by $a^2 m_0^2, b^2 m_0^2, c^2 m_0^2$ respectively. Similar expressions are obtained for the y and z components. This form of the force equations entails evaluation of the elliptic integral R_J for which fast algorithms exist.

The force equations in this simplified notation are then given by

$$\begin{aligned} \mathbf{F}_x &= \frac{2x}{3\pi(1-m_0)} \left[\sum_\tau Q_\tau^A R_J(a^2, b^2, c^2, \tau) - \frac{1}{m_0^2} \sum_{\tau'} Q_{\tau'}^B R_J(a^2, b^2, c^2, \frac{\tau'}{m_0^2}) \right], \\ \mathbf{F}_y &= \frac{2x}{3\pi(1-m_0)} \left[\sum_\tau S_\tau^A R_J(a^2, b^2, c^2, \tau) - \frac{1}{m_0^2} \sum_{\tau'} S_{\tau'}^B R_J(a^2, b^2, c^2, \frac{\tau'}{m_0^2}) \right], \\ \mathbf{F}_z &= \frac{2x}{3\pi(1-m_0)} \left[\sum_\tau T_\tau^A R_J(a^2, b^2, c^2, \tau) - \frac{1}{m_0^2} \sum_{\tau'} T_{\tau'}^B R_J(a^2, b^2, c^2, \frac{\tau'}{m_0^2}) \right]. \end{aligned} \quad (\text{A8})$$

The derivatives of the forces are obtained by differentiating the above expressions for the force. We have

$$\frac{\partial R_J(a^2, b^2, c^2, \tau)}{\partial \tau} = -\frac{3}{2} \int_0^\infty \frac{du}{(u + \tau)^2 \sqrt{(u + a^2)(u + b^2)(u + c^2)}}. \quad (\text{A9})$$

We adopt the notation

$$\tilde{R}_J(\tau) = \frac{\partial R_J(a^2, b^2, c^2, \tau)}{\partial \tau}, \quad (\text{A10})$$

with the understanding that τ represents either the first set of coordinates or τ'/m_0^2 . These improper integrals can be rewritten as proper integrals by a change of variable, $s^2 = a^2/(u + a^2)$, so that

$$\tilde{R}_J(\tau) = \frac{-3}{a^5} \int_0^1 \frac{s^4 ds}{(1 - \hat{\tau} s^2)^2 \sqrt{(1 - \hat{b}^2 s^2)(1 - \hat{c}^2 s^2)}}, \quad (\text{A11})$$

where

$$\hat{\tau} = 1 - \frac{\tau}{a^2}, \quad \hat{b}^2 = 1 - \frac{b^2}{a^2}, \quad \hat{c}^2 = 1 - \frac{c^2}{a^2},$$

and similarly for $\tilde{R}_J(\tau'/m_0^2)$.

Also,

$$\begin{aligned} \frac{\partial Q_\tau^A}{\partial \tau} &= \frac{\partial}{\partial \tau} \left[\frac{(\tau - b^2)(\tau - c^2)}{(\tau - \tau_+)(\tau - \tau_-)} \right] \\ &= \frac{(\tau - b^2)(\tau - c^2)}{(\tau - \tau_+)(\tau - \tau_-)} \left[\frac{1}{(\tau - b^2)} + \frac{1}{(\tau - c^2)} - \frac{1}{(\tau - \tau_+)} - \frac{1}{(\tau - \tau_-)} \right] \end{aligned} \quad (\text{A12})$$

$$\begin{aligned} \frac{\partial Q_{\tau_+}^A}{\partial \tau} &= \frac{\partial}{\partial \tau} \left[\frac{(\tau_+ - b^2)(\tau_+ - c^2)}{(\tau_+ - \tau)(\tau_+ - \tau_-)} \right] \\ &= \frac{Q_{\tau_+}^A}{(\tau_+ - \tau)}. \end{aligned} \quad (\text{A13})$$

Similarly,

$$\frac{\partial Q_{\tau'}^B}{\partial \tau'} = Q_{\tau'}^B \tilde{Q}_{\tau'}^B, \quad (\text{A14})$$

$$\frac{\partial Q_{\tau'_+}^B}{\partial \tau'} = \frac{Q_{\tau'_+}^B}{(\tau'_+ - \tau')}. \quad (\text{A15})$$

With the above notation the force derivatives can be written as

$$\mathbf{F}_{xx} = \frac{\mathbf{F}_x}{x} + \mathbf{F}^A_{xx} + \mathbf{F}^B_{xx} \quad (\text{A16})$$

where

$$\begin{aligned} \mathbf{F}^A_{xx} &= \frac{4x^2}{3\pi(1-m_0)} \left[\sum_\tau (Q_\tau^A)^2 \tilde{Q}_\tau^A R_J(\tau) - \sum_\tau (Q_\tau^A)^2 \tilde{R}_J(\tau) \right. \\ &\quad \left. + \frac{Q_\lambda^A Q_\mu^A}{(\lambda - \mu)} (R_J(\lambda) - R_J(\mu)) + \frac{Q_\mu^A Q_\nu^A}{(\mu - \nu)} (R_J(\mu) - R_J(\nu)) \right. \\ &\quad \left. + \frac{Q_\nu^A Q_\lambda^A}{(\nu - \lambda)} (R_J(\nu) - R_J(\lambda)) \right] \end{aligned} \quad (\text{A17})$$

$$\begin{aligned} \mathbf{F}^B_{xx} &= \frac{-4x^2}{3\pi(1-m_0)m_0^2} \left[\sum_{\tau'} (Q_{\tau'}^B)^2 \tilde{Q}_{\tau'}^B R_J(\tau'/m_0^2) - \frac{1}{m_0^2} \sum_{\tau'} (Q_{\tau'}^B)^2 \tilde{R}_J(\tau'/m_0^2) \right. \\ &\quad \left. + \frac{Q_{\lambda'}^B Q_{\mu'}^B}{(\lambda' - \mu')} (R_J(\lambda'/m_0^2) - R_J(\mu'/m_0^2)) + \frac{Q_{\mu'}^B Q_{\nu'}^B}{(\mu' - \nu')} (R_J(\mu'/m_0^2) - R_J(\nu'/m_0^2)) \right. \\ &\quad \left. + \frac{Q_{\nu'}^B Q_{\lambda'}^B}{(\nu' - \lambda')} (R_J(\nu'/m_0^2) - R_J(\lambda'/m_0^2)) \right]. \end{aligned} \quad (\text{A18})$$

The force derivatives \mathbf{F}_{yy} and \mathbf{F}_{zz} are obtained by substituting $(S_\tau^A, S_{\tau'}^A)$ and $(T_\tau^A, T_{\tau'}^B)$ (A7) in place of $(Q_\tau^A, Q_{\tau'}^A)$ respectively. The cross derivatives of the forces may be written

$$\mathbf{F}_{xy} = \mathbf{F}^A_{xy} + \mathbf{F}^B_{xy}, \quad (\text{A19})$$

$$\begin{aligned} \mathbf{F}^A_{xy} = & \frac{4xy}{3\pi(1-m_0)} \left[\sum_\tau (Q_\tau^A S_\tau^A) \tilde{Q}_\tau^A R_J(\tau) - \sum_\tau (Q_\tau^A S_\tau^A) \tilde{R}_J(\tau) \right. \\ & + \frac{Q_\lambda^A S_\mu^A}{(\lambda - \mu)} (R_J(\lambda) - R_J(\mu)) + \frac{Q_\mu^A S_\nu^A}{(\mu - \nu)} (R_J(\mu) - R_J(\nu)) \\ & \left. + \frac{Q_\nu^A S_\lambda^A}{(\nu - \lambda)} (R_J(\nu) - R_J(\lambda)) \right] \end{aligned} \quad (\text{A20})$$

$$\begin{aligned} \mathbf{F}^B_{xy} = & \frac{-4xy}{3\pi(1-m_0)m_0^2} \left[\sum_{\tau'} (Q_{\tau'}^B S_{\tau'}^B) \tilde{Q}_{\tau'}^B R_J(\tau'/m_0^2) - \frac{1}{m_0^2} \sum_{\tau'} (Q_{\tau'}^B S_{\tau'}^B) \tilde{R}_J(\tau'/m_0^2) \right. \\ & + \frac{Q_{\lambda'}^B S_{\mu'}^B}{(\lambda' - \mu')} (R_J(\lambda'/m_0^2) - R_J(\mu'/m_0^2)) + \frac{Q_{\mu'}^B S_{\nu'}^B}{(\mu' - \nu')} (R_J(\mu'/m_0^2) - R_J(\nu'/m_0^2)) \\ & \left. + \frac{Q_{\nu'}^B S_{\lambda'}^B}{(\nu' - \lambda')} (R_J(\nu'/m_0^2) - R_J(\lambda'/m_0^2)) \right]. \end{aligned} \quad (\text{A21})$$

Similar expressions may be obtained for \mathbf{F}_{yz} and \mathbf{F}_{zx} .

A high degree of speed and accuracy were desired for the orbit integration routines. The accuracy with which the forces are computed and consequently the speed of the orbital integration depends crucially on the accuracy with which the ellipsoidal coordinates (λ, μ, ν) are calculated. The requisite accuracy could always be obtained using the NAG routine C02AGF for finding the roots of a polynomial equation; however these root evaluations were computationally expensive. Therefore for large values of the constant m_0 the roots were computed from standard algebraic expressions for the roots of a cubic equation (e.g. Press et al. 1987). When m_0 is small the algebraic expressions to evaluate the roots (λ', μ', ν') do not yield the required accuracy and the NAG routines are essential.

A great increase in the speed of evaluation of the forces was obtained by fitting cubic splines (NAG routine E01BAF) to the elliptic integrals $R_J(\tau)$, $R_J(\tau'/m_0^2)$ and their derivatives $\tilde{R}_J(\tau)$, $\tilde{R}_J(\tau'/m_0^2)$. τ lies in the range $c^2 \leq \tau \leq a^2 \leq \lambda_{max}$ and $m_0^2 c^2 \leq \tau' \leq m_0^2 a^2 \leq \lambda'_{max}$, where λ_{max} and λ'_{max} are the maximum values of the ellipsoidal coordinates λ and λ' which depend on the maximum values of the cartesian coordinates (x^2, y^2, z^2) . The integral are first tabulated over the range $[c^2, \lambda_{max}/m_0^2]$ at the start of the orbit integration and are evaluated by a cubic spline interpolant (NAG routine E02BBF) thereafter. The functions $R_J(\tau)$, $R_J(\tau'/m_0^2)$, $\tilde{R}_J(\tau)$ and $\tilde{R}_J(\tau'/m_0^2)$ increase steeply as τ

decreases for small values of τ and it was found that the accuracy of interpolation could be greatly improved by multiplying the functions by powers of τ and τ'/m_0^2 respectively. The actual functions that were splined were therefore: $[(\tau)^{3/4}R_J(\tau)]$, $[(\tau'/m_0^2)^{3/4}R_J(\tau'/m_0^2)]$ and $[(\tau)^{3/2}\tilde{R}_J(\tau)]$, $[(\tau'/m_0^2)^{3/2}\tilde{R}_J(\tau'/m_0^2)]$. This procedure yielded a value of the true functions which was accurate to at least 14 figures.

The potential due to a central black hole of mass M_{BH} at a radius R from the center is $\Phi^{BH} = -GM_{BH}/R$. In cartesian coordinates the forces at a point (x_1, x_2, x_3) (with $R^2 = \sum_{i=1,3} x_i^2$ and $G = 1$) are given by

$$F_{x_i}^{BH} = \frac{-M_{BH}x_i}{R^3} \quad (A22)$$

The corresponding force derivatives are

$$F_{x_i x_j}^{BH} = \frac{-M_{BH}}{R^5}(\delta_{ij}R^2 - 3x_i x_j) \quad (A23)$$

REFERENCES

Arnold, V. I. 1964, Russian Math. Surveys, 18, 85

Arnold, V. I. 1989, Mathematical Methods of Classical Mechanics (New York: Springer)

Arnold, V. I. & Avez, A. 1968, Ergodic Problems of Classical Mechanics (New York: Benjamin)

Benettin, G., Galgani, L., Giorgilli, A. & Strelcyn, J.-M. 1980, Meccanica, 15, 21

Binney, J. J. 1982a, MNRAS, 201, 1

Binney, J. J. 1982b, MNRAS, 201, 15

Binney, J. J. & Tremaine, S. 1987, Galactic Dynamics (Princeton University Press), 220

Chandrasekhar, S. 1969, Ellipsoidal Figures of Equilibrium (New York: Dover), 52

Crane, P., *et al.* 1993, AJ, 106, 1371

Davies, R. *et al.* 1983, ApJ, 266, 41

Dehnen, W. 1993, MNRAS, 265, 250

Dehnen, W. 1995, MNRAS, 274, 919

Dehnen, W. 1996, private communication

Dejonghe, H. 1987, ApJ, 320, 477

de Zeeuw, P. T. 1985, MNRAS, 216, 273

de Zeeuw, P. T. 1994, Lecture Notes of the Canary Islands Winter School, “Formation of Galaxies.”

de Zeeuw, P. T. & Lynden-Bell, D. 1985, MNRAS, 215, 713

de Zeeuw, P. T. & Pfenniger, D. 1988, MNRAS, 235, 949

Ferrarese, L., van den Bosch, F. C., Ford, H. C., Jaffe, W., & O’Connell, R. W. 1994, AJ, 108, 1598

Ford, H. C. *et al.* 1994, ApJL 435, L27

Franx, M., Illingworth, G. & de Zeeuw, T. 1991, ApJ, 383, 112

Gebhardt, K. *et al.* 1996, preprint

Gerhard, O. E. 1993, 6th European EADN Summer School: Galactic Dynamics and N-Body Simulations, ed. G. Contopoulos & G. Spyrou (New York: Springer)

Gerhard, O. E. & Binney, J. J. 1985, MNRAS, 216, 467

Goodman, J. & Schwarzschild, M. 1981, ApJ, 245, 1087

Habib, S., Kandrup, H. E., & Mahon, M. E. 1995, Phys. Rev. E, in press

Hubble, E. W. 1930, ApJ, 71, 231

Jeans, J. J. 1915, MNRAS, 76, 71

Kandrup, H. E. & Mahon, M. E. 1994, Phys. Rev. E, 49, 3735

Karney, C. F. F. 1983, Physica 8D, 360

Katz, N. & Richstone, D. O. 1985, ApJ, 296, 331

Kormendy, J., *et al.* 1995, ESO/OHP Workshop on Dwarf Galaxies, ed. G. Meylan & P. Prugniel (Garching: ESO), 147

Kormendy, J. & Bender, R. 1996, preprint

Kormendy, J. & Richstone, D. 1995, Ann. Rev. Astron. Astrophys., 33, 581

Krylov, N. S. 1979, Works on the Foundations of Statistical Physics (Princeton University Press)

Kuzmin, G. G. 1973, The Dynamics of Galaxies and Star Clusters, ed. T. B. Omarov (Nauka of the Kazakh S. S. R., Alma-Ata), 71.

Lauer, T., *et al.* 1995, AJ, 110, 2622

Lichtenberg, A. J. & Lieberman, M. A. 1983, Regular and Stochastic Motion (New York: Springer)

Lynden-Bell, D. 1967, MNRAS, 136, 101

Mackay, R. S., Meiss, J. D. & Percival, I. C. 1984, Physica 13D, 55

Mahon, M. E., Abernathy, R. A., Bradley, B. O. & Kandrup, H. E. 1995, MNRAS, 275, 443

Merritt, D. 1980, ApJ Suppl., 43, 435

Merritt, D. & Fridman, T. 1995, A. S. P. Conf. Ser. Vol. 86, Fresh Views of Elliptical Galaxies, ed. A. Buzzoni, A. Renzini & A. Serrano (Provo: Astronomical Society of the Pacific), 13

Merritt, D. & Fridman, T. 1996, ApJ, 460, 136

Miralda-Escude, J. & Schwarzschild, M. 1989, ApJ, 339, 752

Miyoshi, M., Moran, J., Herrnstein, J., Greenhill, L., Nakai, N., Diamond, P. & Inoue, M. 1995, Nature, 373, 127

Moller, P., Stiavelli, M. & Zeilinger, W. W. 1995, MNRAS, 276, 979

Ott, E. 1993, Chaos in Dynamical Systems (Cambridge University Press), 257

Schwarzschild, M. 1981, The Structure and Evolution of Normal Galaxies, ed. S. M. Fall & D. Lynden-Bell (Cambridge University Press), 43

Schwarzschild, M. 1987, *Ann. N. Y. Acad. Sci.*, 497, 16

Schwarzschild, M. 1993, *ApJ*, 409, 563

Sinai, Ya. G. 1976, Introduction to Ergodic Theory (Princeton University Press)

Spitzer, L. & Hart, M. 1971, *ApJ*, 164, 399

Tonry, J. L. 1987, *ApJ*, 322, 632

Tremblay, B. & Merritt, D. 1996, *AJ*, 111, 000

Udry, S. & Pfenniger, D. 1988, *AAp*, 198, 135

van der Marel, R. P., Evans, N. W., Rix, H. W., White, S. D. M. & de Zeeuw, T. 1994, *MNRAS*, 271, 99

Fig. 1.—

Phase-mixing (a) vs. chaotic mixing (b).

Fig. 2.—

Density law (5), for $m_0 = 0, 0.002, 0.005, 0.01, 0.02, 0.05, 0.1, 0.2, 0.5, 1$. Heavy lines are profiles with the three values of m_0 used in the potentials studied here.

Fig. 3.—

Histograms of Liapunov numbers for isoenergetic ensembles of boxlike orbits in the triaxial potential of Eq. (8), with $m_0 = 10^{-1}$ (a), $m_0 = 10^{-2}$ (b) and $m_0 = 10^{-3}$ (c). $c/a = 0.5$ and $b/a = 0.79$. Heavy lines: $t = 10^4 T_D$; intermediate lines: $t = 10^3 T_D$; thin lines: $t = 10^2 T_D$.

Fig. 4.—

Histograms of Liapunov numbers for isoenergetic ensembles of boxlike orbits in the triaxial potential of Eq. (8), with $m_0 = 10^{-1}$ and $M_{BH} = 10^{-3}$ (a), 3×10^{-3} (b) and 10^{-2} (c). $c/a = 0.5$ and $b/a = 0.79$. Heavy lines: $t = 10^4 T_D$; intermediate lines: $t = 10^3 T_D$; thin lines: $t = 10^2 T_D$.

Fig. 5.—

Histograms of Liapunov numbers for isoenergetic ensembles of boxlike orbits in the triaxial potential of Eq. (8), with $m_0 = 10^{-3}$ and $M_{BH} = 10^{-3}$ (a), 3×10^{-3} (b) and 10^{-2} (c). $c/a = 0.5$ and $b/a = 0.79$. Heavy lines: $t = 10^4 T_D$; intermediate lines: $t = 10^3 T_D$; thin lines: $t = 10^2 T_D$.

Fig. 6.—

Velocities at central crossings ($x \approx y \approx z \approx 0$) for boxlike orbits in three models. The dots in this velocity octant map mark the velocity at one near-center passage. (a) $M_{BH} = 0$. Large dots: $m_0 = 10^{-1}$; medium dots: $m_0 = 10^{-2}$; small dots: $m_0 = 10^{-3}$. (b) $m_0 = 10^{-1}$. Large dots: $M_{BH} = 10^{-3}$; medium dots: $M_{BH} = 3 \times 10^{-3}$; small dots: $M_{BH} = 10^{-2}$.

Fig. 7.—

Starting points of boxlike orbits on one octant of the equipotential surface. Small dots are stochastic orbits; large dots are regular orbits; circles are trapped stochastic orbits. (a) $m_0 = 10^{-3}$, $M_{BH} = 0$ (Model 1). (b) $m_0 = 10^{-1}$, $M_{BH} = 3 \times 10^{-3}$ (Model 2). Numbers denote starting points of the ensembles used in the mixing experiments of §5.

Fig. 8.—

Evolution of Ensemble No. 4 in Model 1 ($m_0 = 10^{-3}$, $M_{BH} = 0$). Plotted are projections onto the $x - z$ plane of the configuration-space density of 10^4 , independently-moving points. Numbers are the elapsed time in units of T_D . Tick marks are separated by one length unit.

Fig. 9.—

Cuts through the principal planes of the ensemble densities at $t = 200T_D$. (a) Ensemble No. 1, Model 1. (b) Ensemble No. 1, Model 2.

Fig. 10.—

Evolution of F , the fraction of configuration-space cells containing no particles, for the 12 mixing ensembles. (a) Model 1 ($m_0 = 10^{-3}$, $M_{BH} = 0$); (b) Model 2 ($m_0 = 10^{-1}$, $M_{BH} = 3 \times 10^{-3}$). Dotted lines are trapped ensembles.

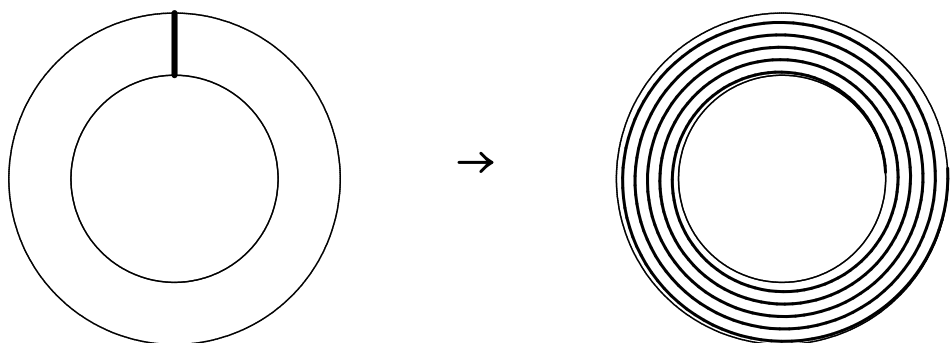
Fig. 11.—

Evolution of D_1 , the “distance” between the ensemble density and the micro-canonical density, for the 12 mixing ensembles without noise. (a) Model 1 ($m_0 = 10^{-3}$, $M_{BH} = 0$); (b) Model 2 ($m_0 = 10^{-1}$, $M_{BH} = 3 \times 10^{-3}$). Dotted lines are trapped ensembles.

Fig. 12.—

Evolution of D_1 , the “distance” between the ensemble density and the micro-canonical density, for the 12 mixing ensembles with noise, $\eta = 10^4$. (a) Model 1 ($m_0 = 10^{-3}$, $M_{BH} = 0$); (b) Model 2 ($m_0 = 10^{-1}$, $M_{BH} = 3 \times 10^{-3}$). Dotted lines are trapped ensembles.

(a)



(b)

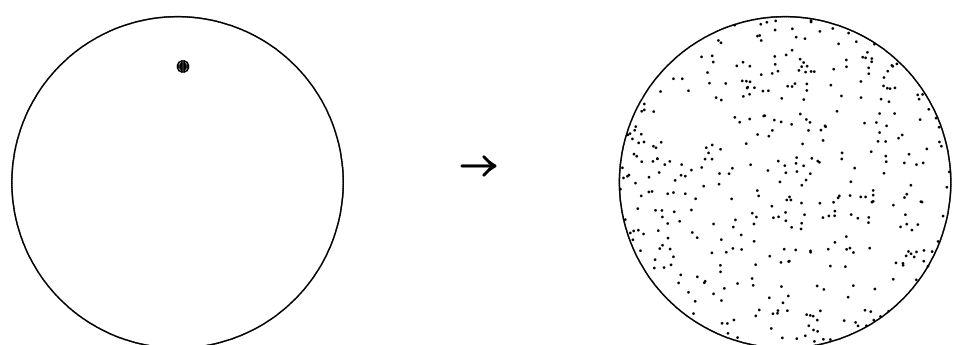


Fig. 1.—

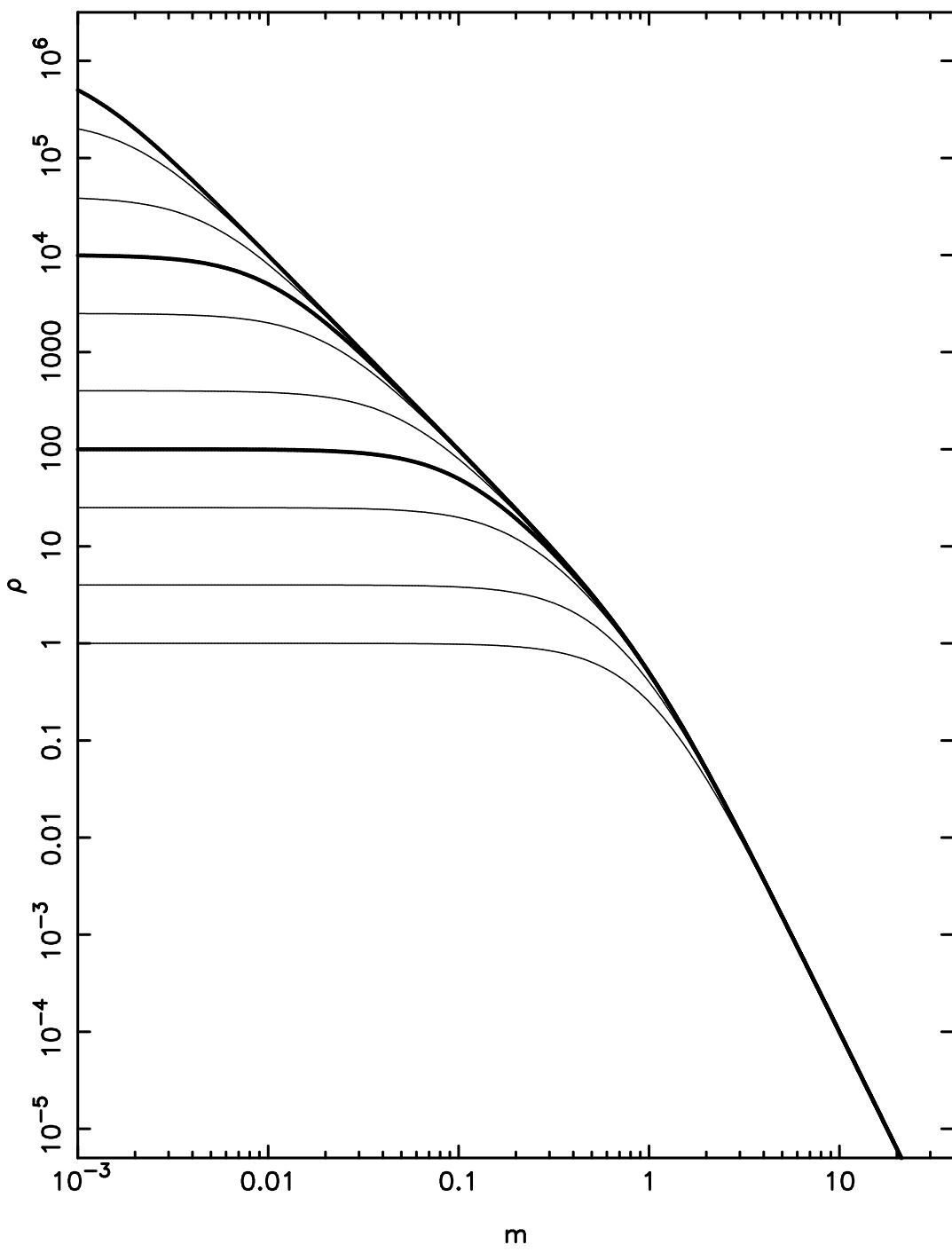


Fig. 2.—

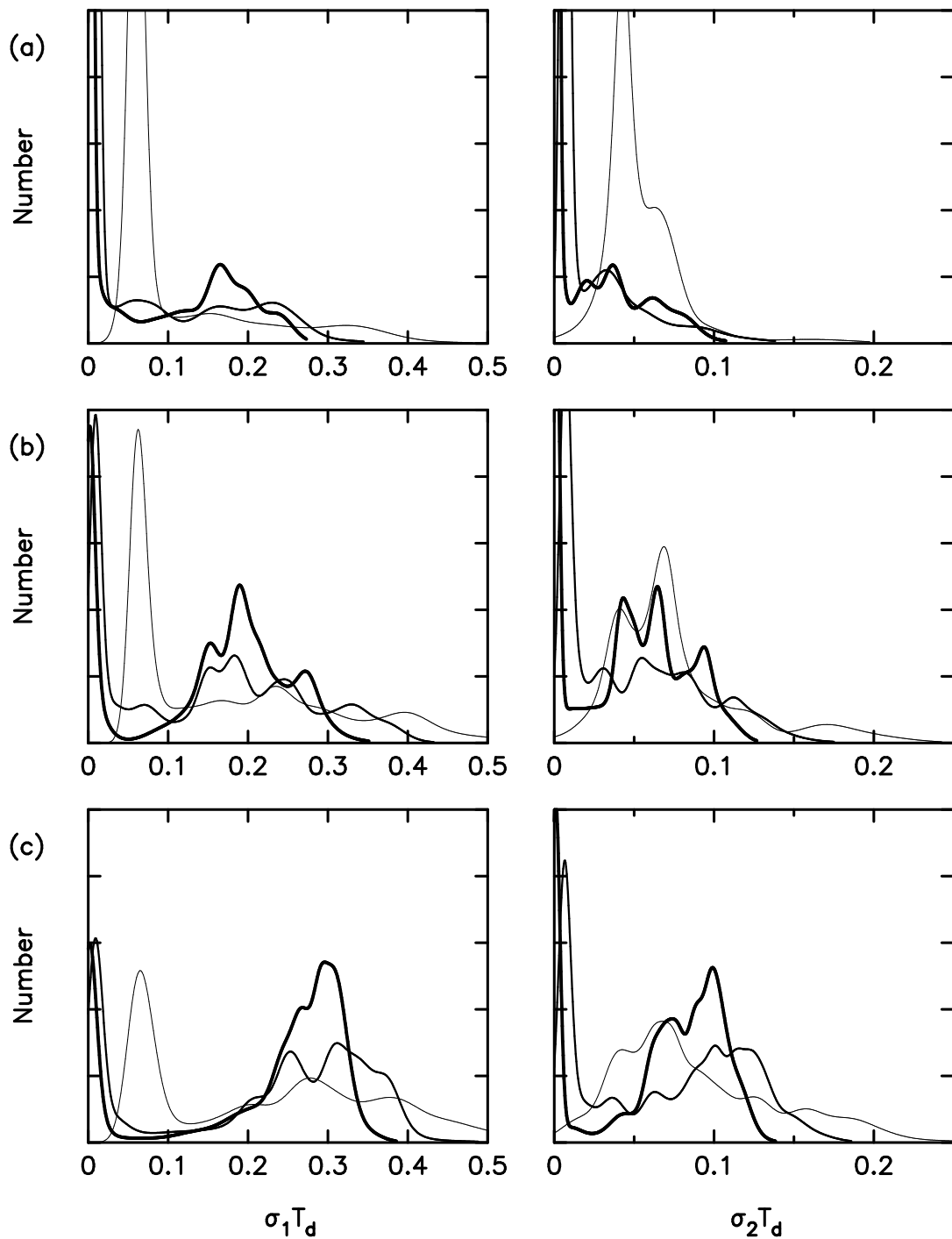


Fig. 3.—

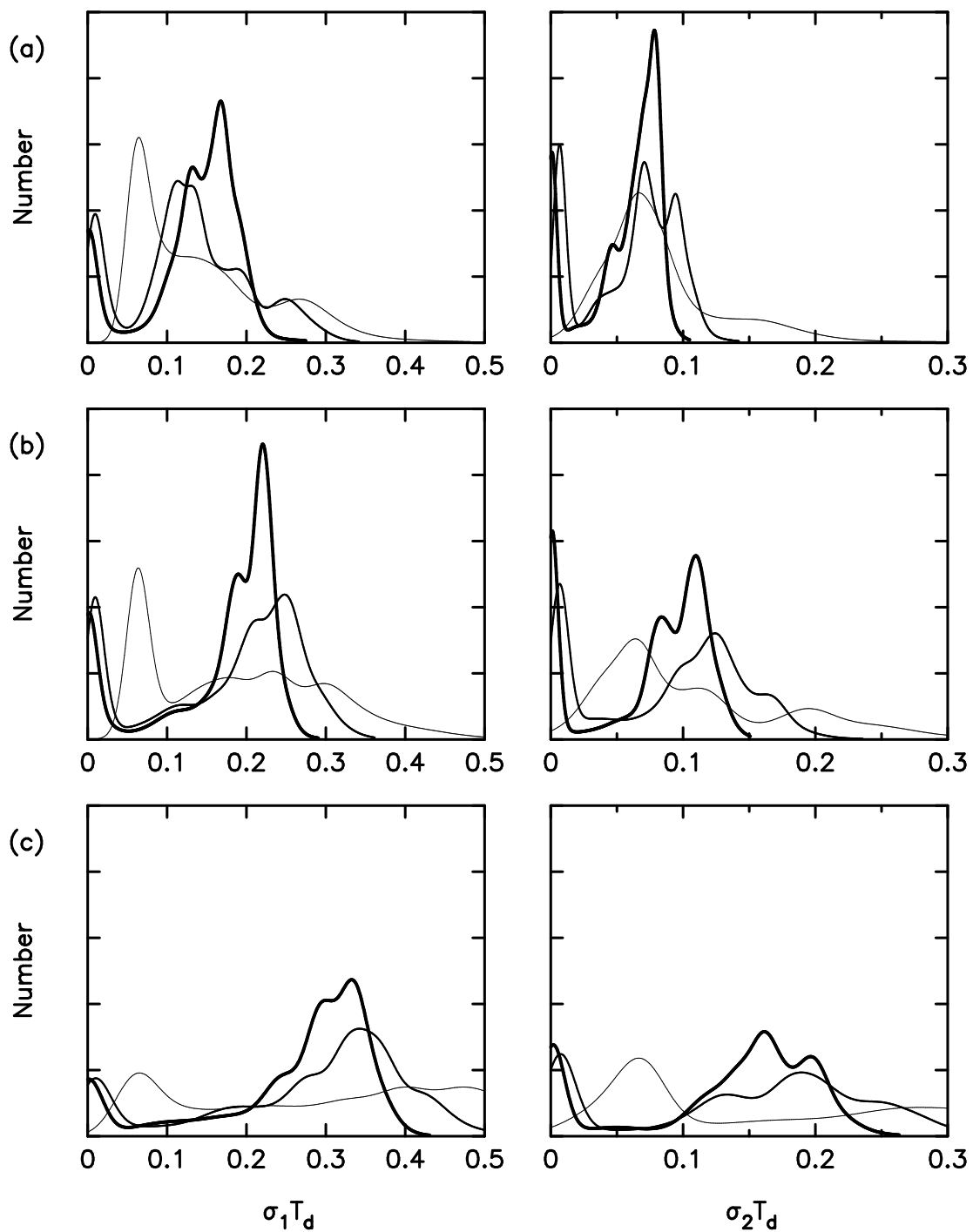


Fig. 4.—

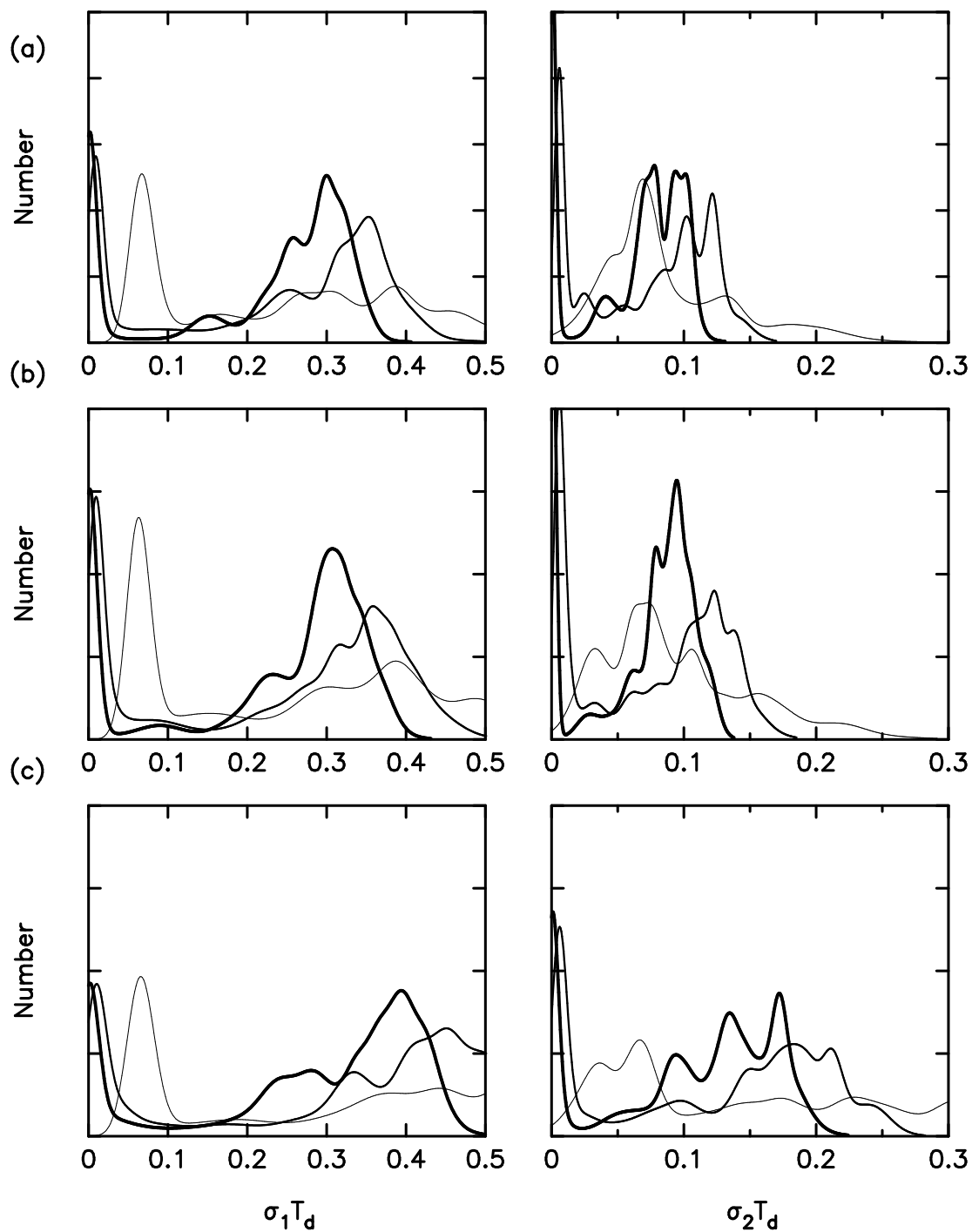


Fig. 5.—

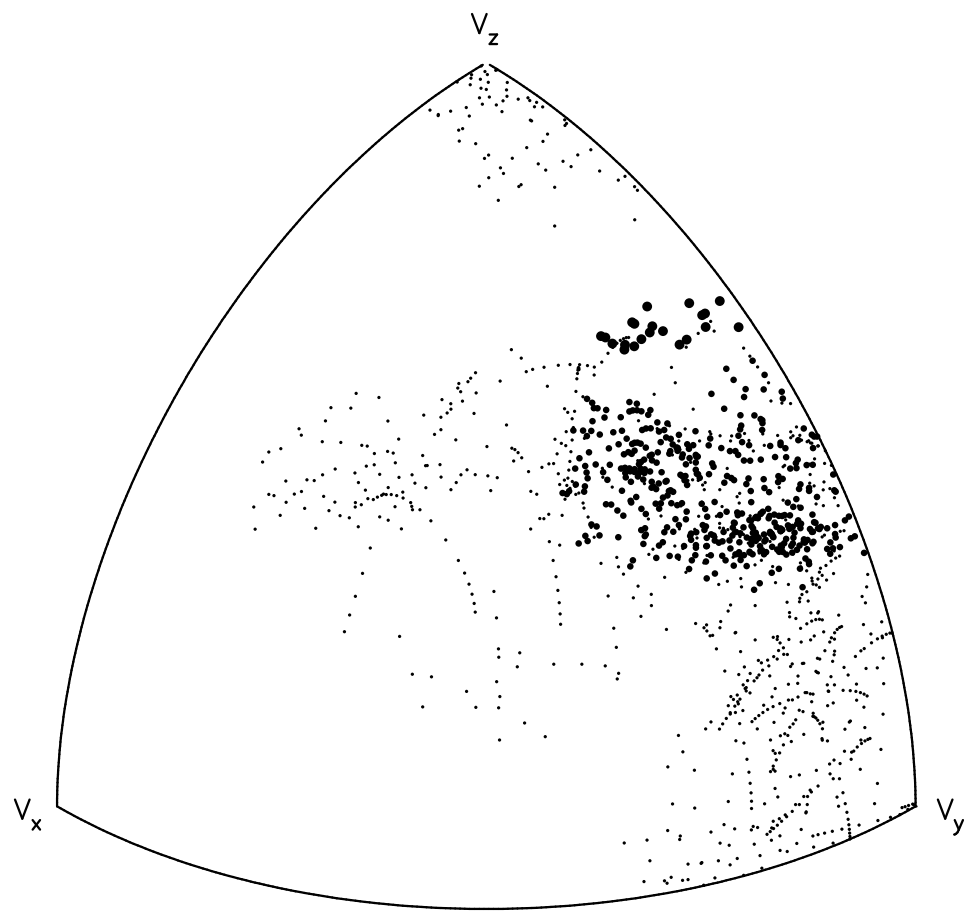


Fig. 6.—

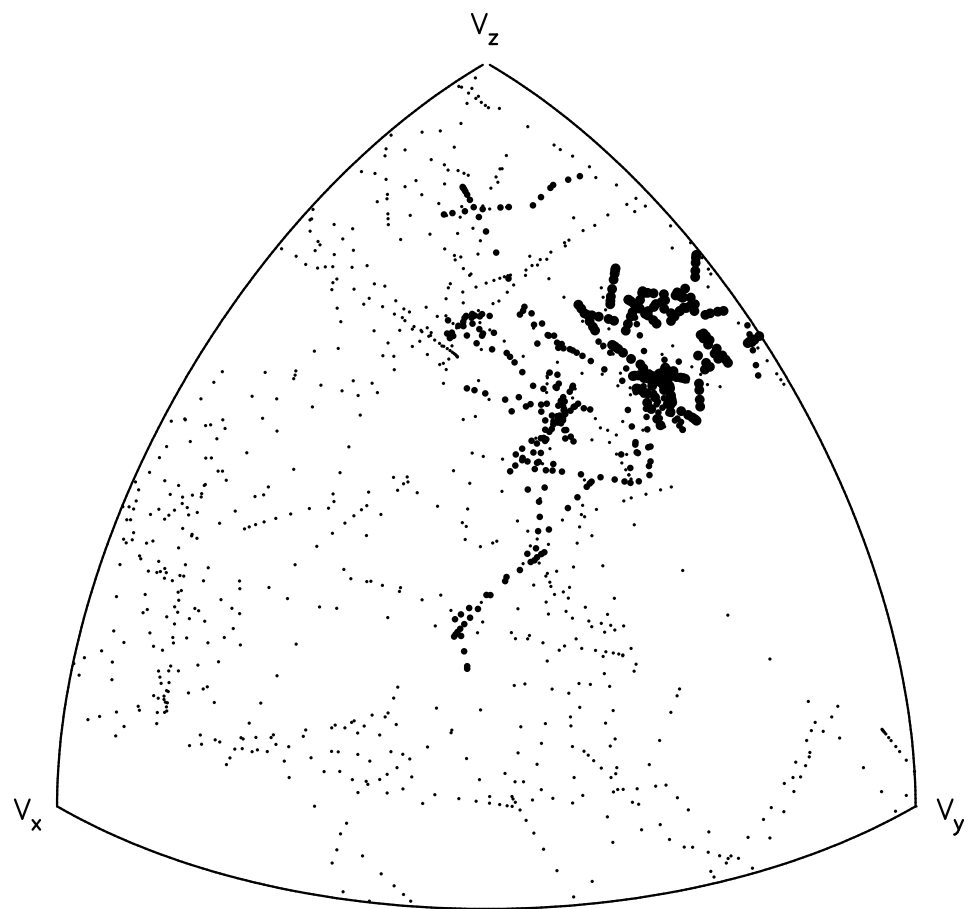


Fig. 6.—

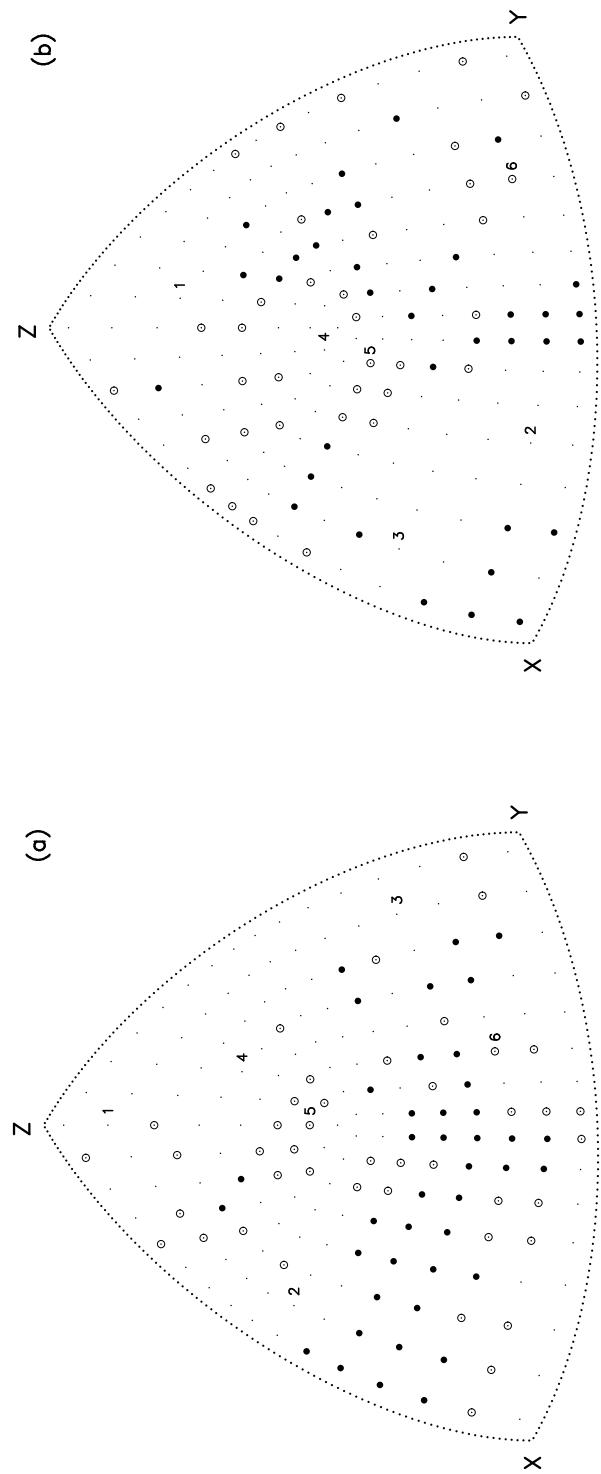


Fig. 7.—

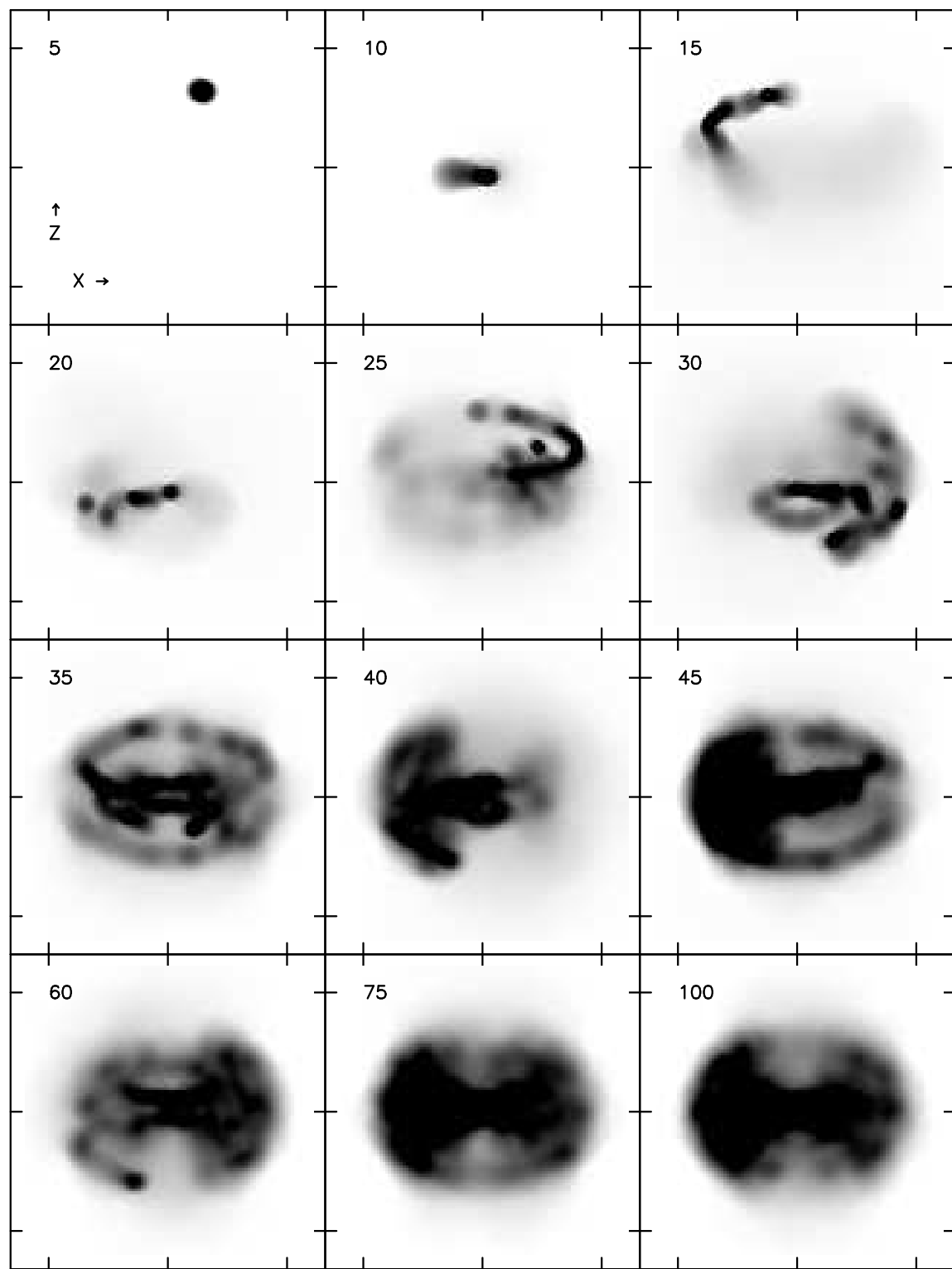


Fig. 8.—

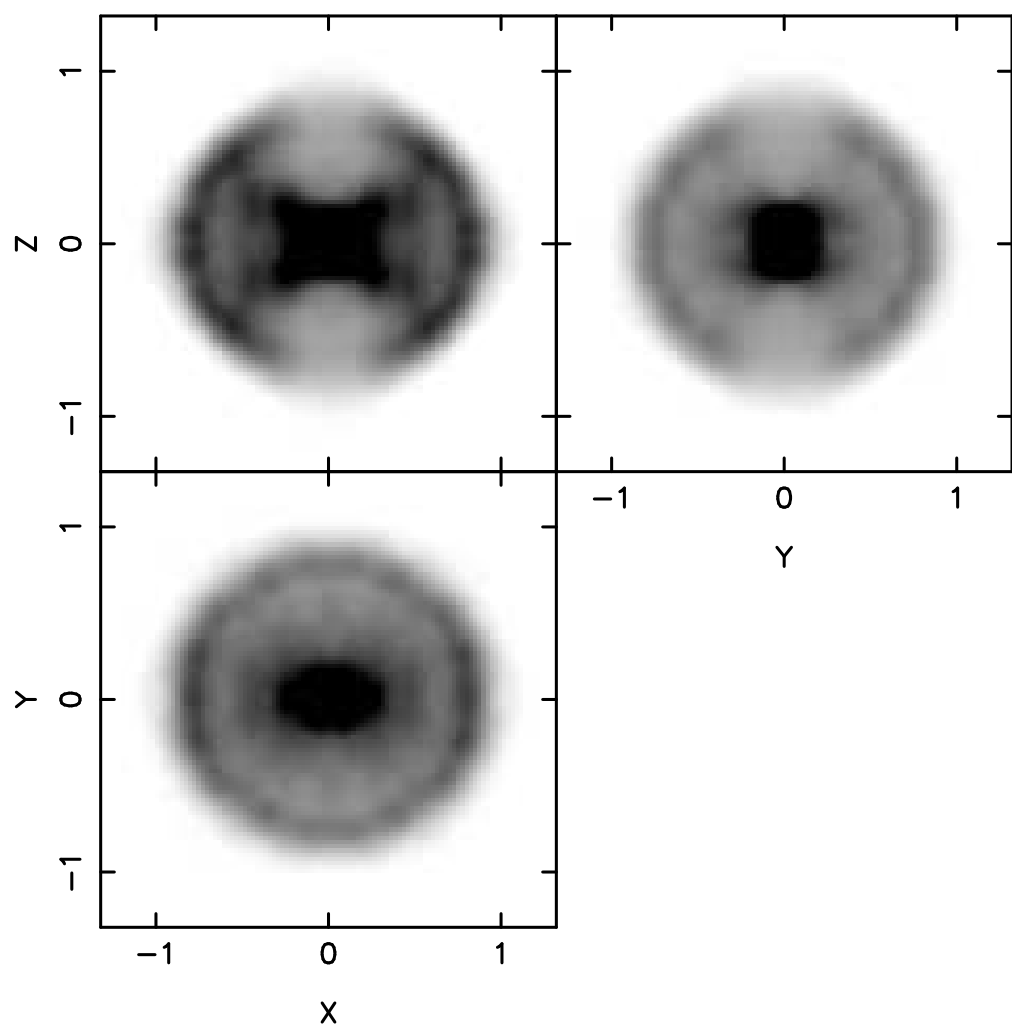


Fig. 9.—

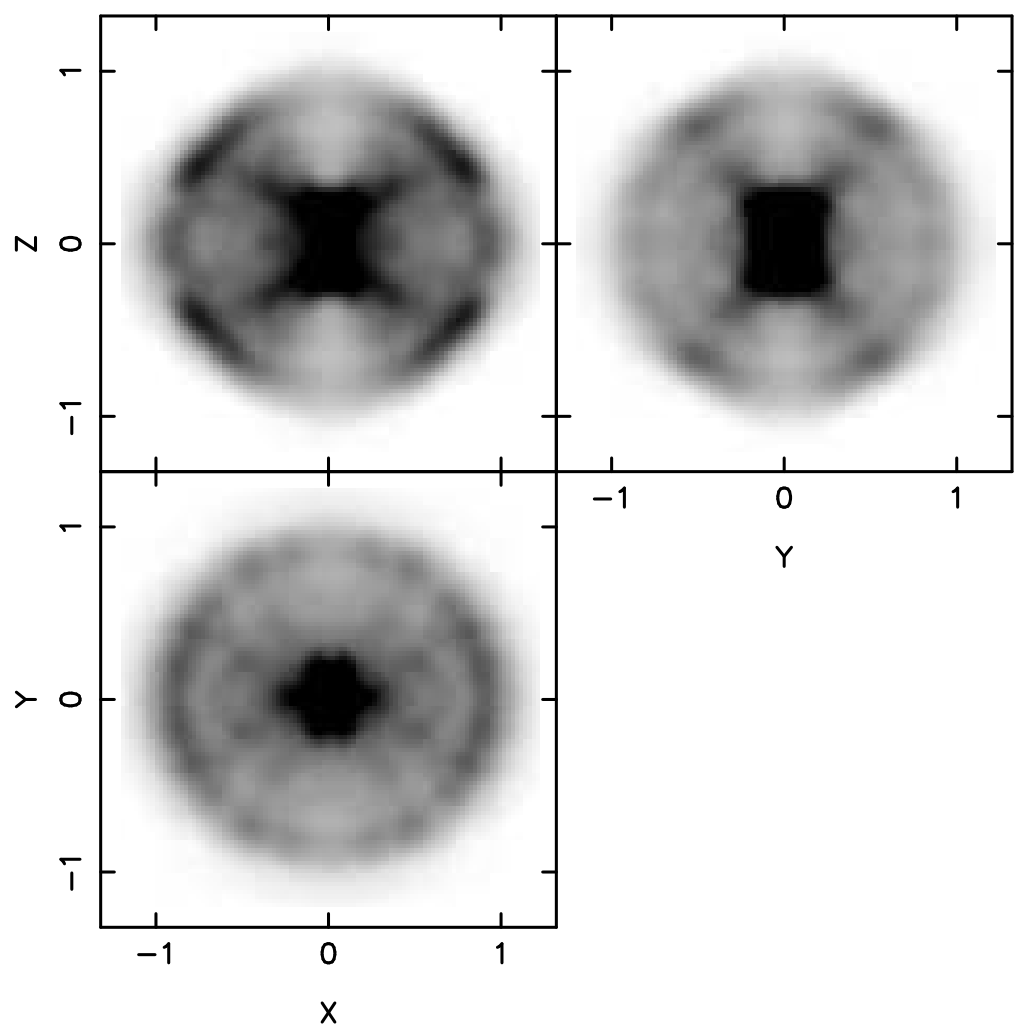


Fig. 9.—

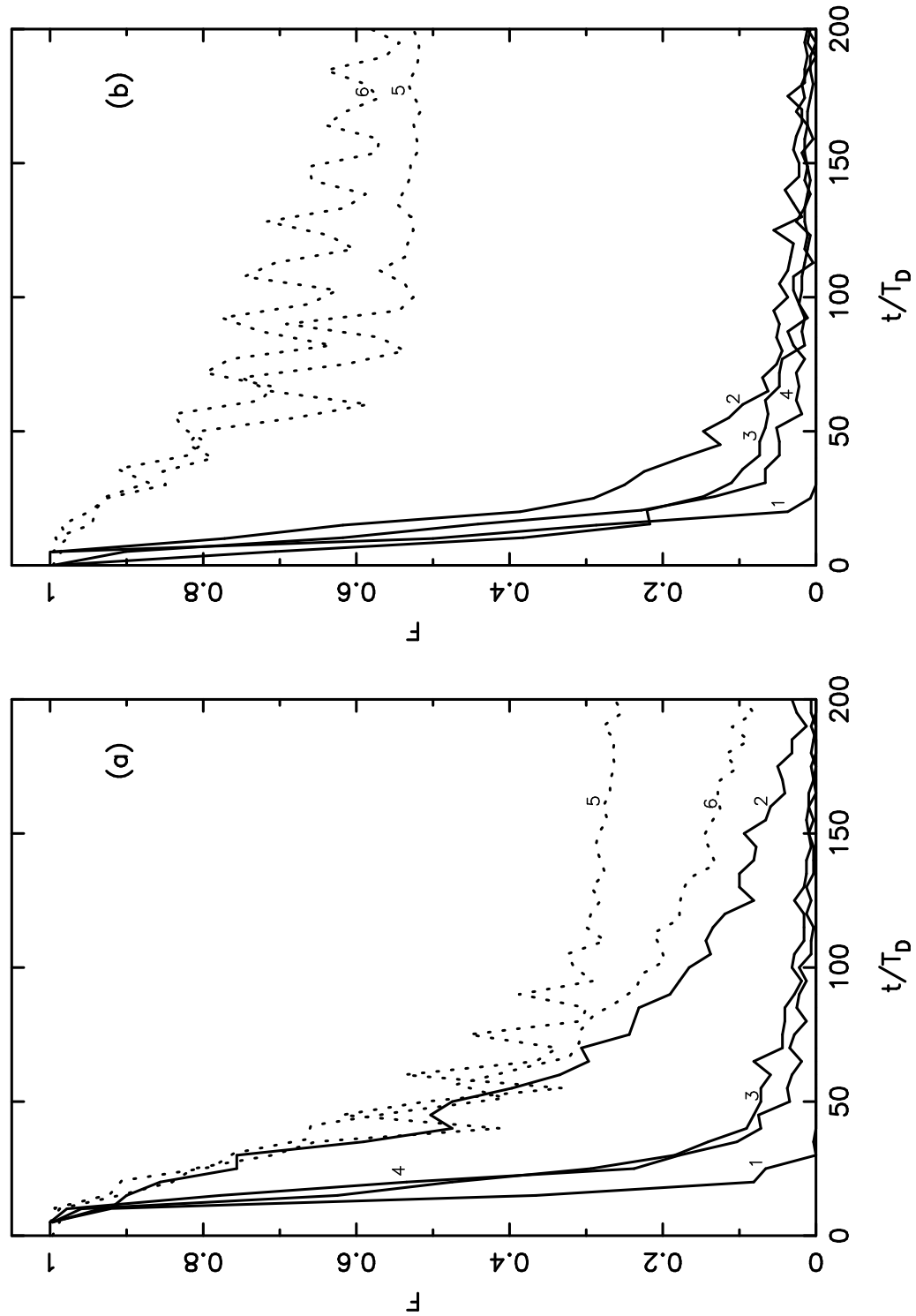


Fig. 10.—

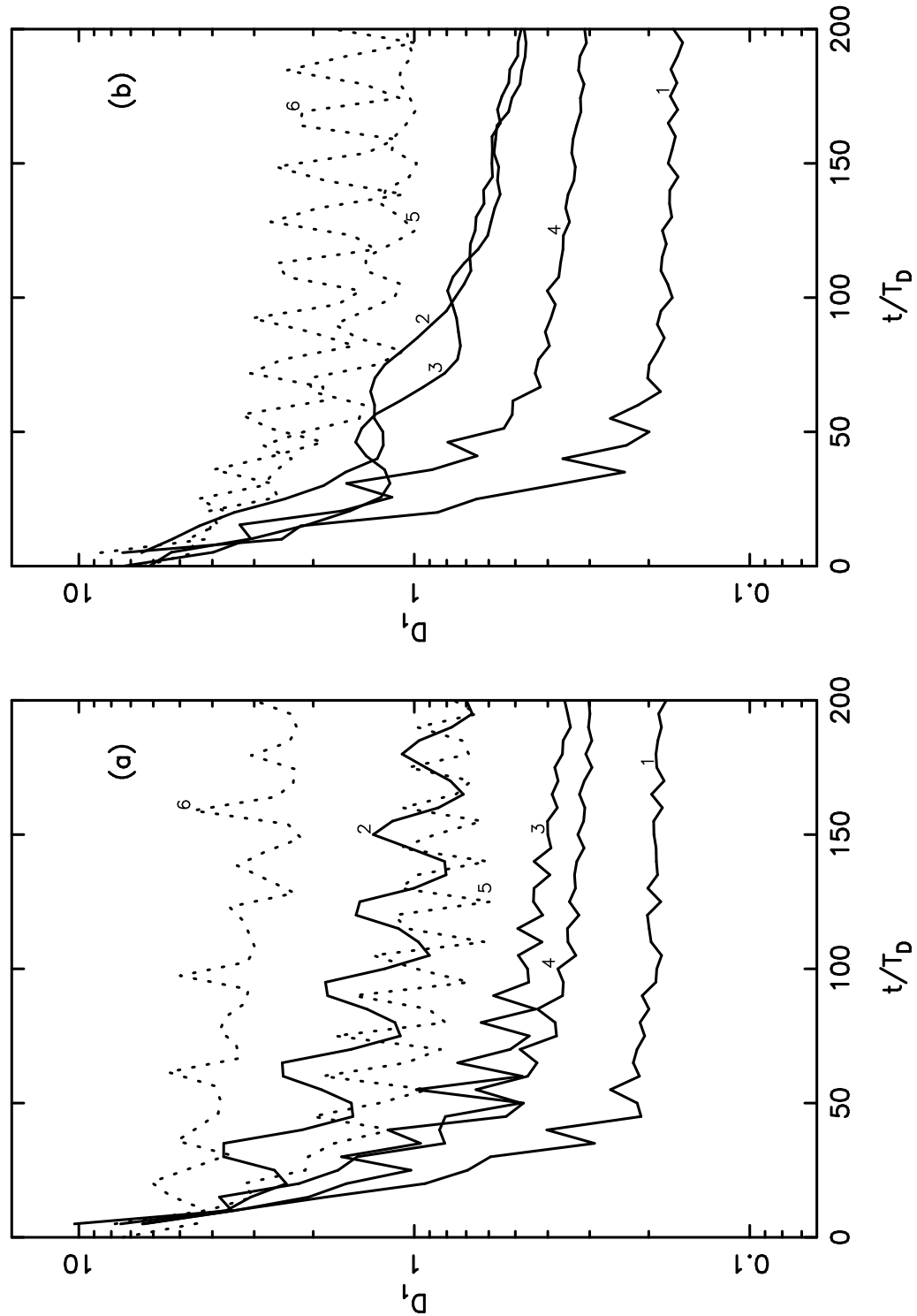


Fig. 11.—

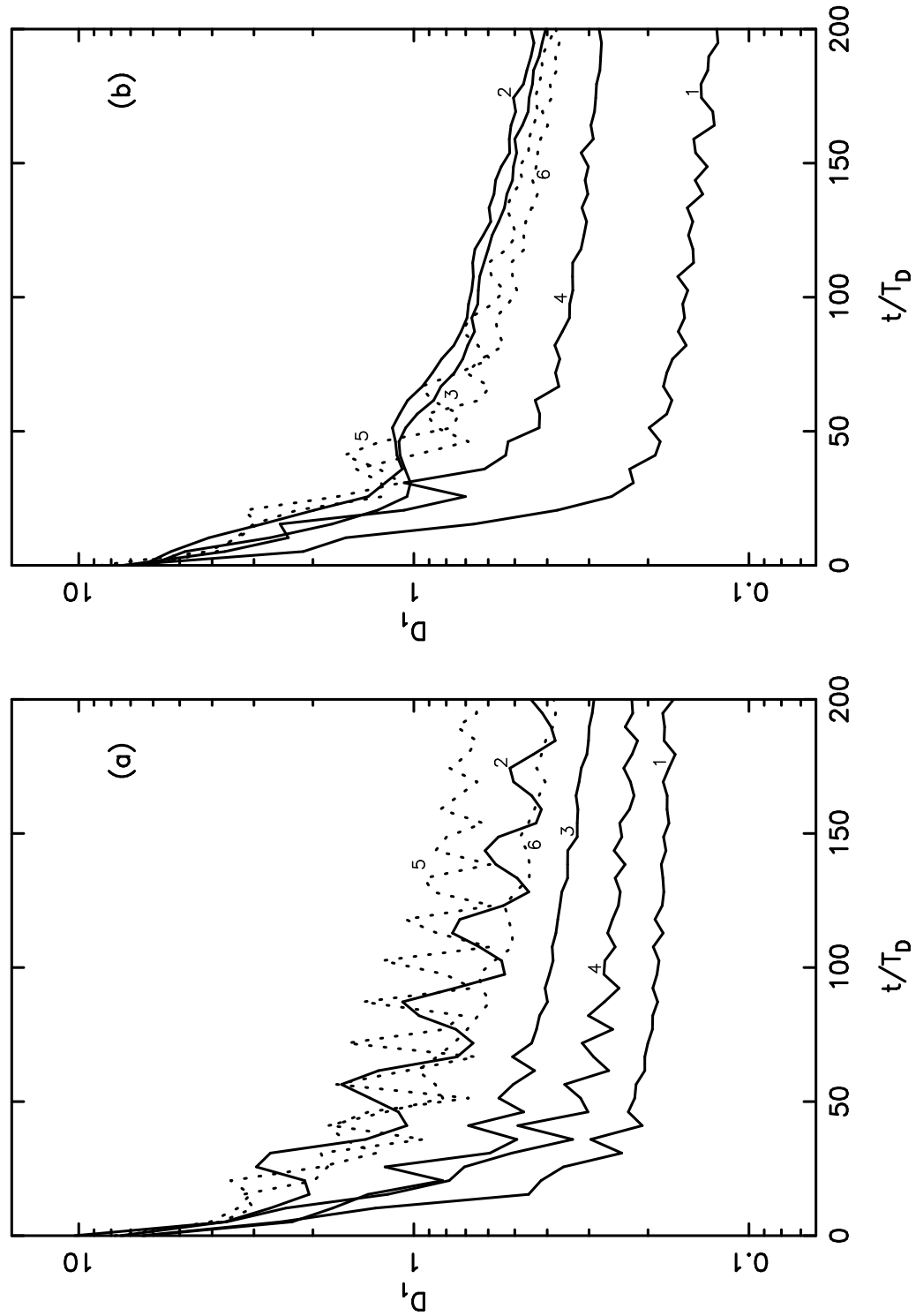


Fig. 12.—